



Review

Magnesium alloys in tumor treatment: Current research status, challenges and future prospects

Yuchien Hsu^{a,b,1}, Yupu Lu^{b,c,1}, Siyi Wang^{a,b,d,1}, Yufeng Zheng^{e,*}, Dandan Xia^{b,c,**},
Yunsong Liu^{a,b,***}

^aDepartment of Prosthodontics, Peking University School and Hospital of Stomatology, Beijing, 100081, China

^bNational Center for Stomatology, National Clinical Research Center for Oral Diseases, National Engineering Research Center of Oral Biomaterials and Digital Medical Devices, Beijing Key Laboratory of Digital Stomatology, Research Center of Engineering and Technology for Computerized Dentistry Ministry of Health, NMPA Key Laboratory for Dental Materials, Beijing, 100081, China

^cDepartment of Dental Materials, Peking University School and Hospital of Stomatology, Beijing, 100081, China

^dDepartment of Prosthodontics, Shanghai Ninth People's Hospital, Shanghai Jiao Tong University School of Medicine, College of Stomatology, Shanghai Jiao Tong University, National Center for Stomatology, National Clinical Research Center for Oral Diseases, Shanghai Key Laboratory of Stomatology, Shanghai Research Institute of Stomatology, China

^eDepartment of Materials Science and Engineering, College of Engineering, Peking University, Beijing 100871, China

Received 8 June 2023; received in revised form 9 August 2023; accepted 13 August 2023

Available online 12 October 2023

Abstract

Cancer is a major threat to human life worldwide. Traditional cancer treatments, such as chemotherapy and surgery, have major limitations and can cause irreversible damage to normal tissues while killing the cancer cells. Magnesium (Mg) alloys are widely reported novel potential biomedical materials with acceptable mechanical properties and good osteogenic and angiogenic properties. In this review, we summarize the Mg alloys for antitumor applications, including pure Mg and Mg alloys (Mg-Ag, Mg-Gd, Mg-Li-Zn, Mg-Ca-Sr-Zn, et al.) fabricated by casting and extruding, selective laser melting methods. Mg alloys can exhibit antitumor effect on bone tumor, breast cancer, and liver tumor, et al. What's more, after tumor tissue is eliminated, Mg alloys prevent tumor recurrence, fill tissue defects and promote tissue regeneration. The antitumor effects of Mg alloys are mainly due to their degradation products. Overall, Mg alloys show great potential in tumor treatments due to the dual function of antitumor and tissue regeneration.

© 2023 Chongqing University. Publishing services provided by Elsevier B.V. on behalf of KeAi Communications Co. Ltd.

This is an open access article under the CC BY-NC-ND license (<http://creativecommons.org/licenses/by-nc-nd/4.0/>)

Peer review under responsibility of Chongqing University

Keywords: Antitumor; Cancer; Magnesium alloys; Mechanism; Tissue regeneration.

1. Introduction

Cancer is a major threat to human life worldwide. Currently, the main cancer treatments include chemotherapy, radiotherapy, and surgical excision of lesions. These traditional treatment methods have certain limitations, such as high surgical risk and trauma during treatment, severe adverse reactions, and a lack of specificity for radiotherapy, which can also damage healthy tissues [1,2]. There is growing interest in exploring alternative therapies that are more targeted and less harmful to healthy tissues. Researchers have been striving to develop more effective therapies to fight cancer,

* Corresponding author at: School of Materials Science and Engineering, Peking University, No.5 Yi-He-Yuan Road, HaiDian District, Beijing 100871, China.

** Corresponding author at: Department of Dental Materials, Peking University School and Hospital of Stomatology, No.22. Zhongguancun South Avenue, Haidian District, Beijing 100081, China.

*** Corresponding author at: Department of Prosthodontics, Peking University School and Hospital of Stomatology, No.22. Zhongguancun South Avenue, Haidian District, Beijing 100081, China.

E-mail addresses: yfzheng@pku.edu.cn (Y. Zheng), dandanxia@pku.edu.cn (D. Xia), liuyunsong@hsc.pku.edu.cn (Y. Liu).

¹ These authors contributed equally to this work.

given its high mortality rates. Many new cancer therapies are emerging, including (but not limited to) gene therapy [3,4], immunotherapy [5,6], and hyperthermia [7], all of which may improve treatment outcomes.

Nevertheless, the current methods of treating tumors are still relatively limited, and there is still a long way to go to achieve cures for all cancers. It is important to develop novel biomaterials that can simultaneously inhibit tumor cells without damaging healthy tissues. Much effort has been expended exploring next-generation biodegradable materials with clinical potential; one such approach is the use of magnesium (Mg) alloys in cancer treatment [8,9].

Mg-based biodegradable metals (BMs) are promising biomaterials for biomedical applications, due to their high biodegradability and good mechanical and biocompatibility properties [10]. Mg has various biological functions in energy metabolism, macromolecule synthesis, and the expression of genetic information [11,12]. Studies have confirmed the surgical success and tolerance of Mg-based absorbable metal stents in different coronary and pulmonary arteries and lower extremity vessels [13]. Besides, Mg and its alloys are considered as potential materials for bone repair applications due to close elastic modulus to human bone, essential nutrient element, high mechanical properties, and good biocompatibility [10,14–16]. Mg^{2+} can promote osteogenic differentiation has also been well proved both *in vitro* and *in vivo* experiments [17].

In recent years, researchers are exploring new functions of Mg alloys. It was reported that the byproducts of Mg alloys, including H_2 , Mg^{2+} , and $Mg(OH)_2$, exhibited significant antitumor effects [18]. Some studies have applied Mg alloys in osteosarcoma (OS) [19–31], breast [8,32–35], ovarian [36], prostate [37], colon [38,39], gallbladder [40], liver [41], and other cancers and confirmed their antitumor and anti-recurrence effects. Moreover, Mg alloys can promote tissue healing, which can fill the tissue defect after a tumor is eliminated, promoting healthy tissue regeneration, and improving patient prognosis.

This review focus on the Mg alloys developed for anti-tumor applications, summarizes the tumor in different sites of the body. Furthermore, the mechanisms of Mg alloys on tumor inhibition are discussed. Finally, we comments on the remaining challenges and perspectives of Mg alloys in cancer treatment.

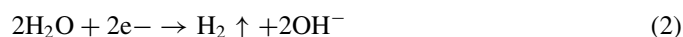
2. Biological characteristics of tumors

A tumor is a collection of local cells with abnormal morphology and function under the action of various carcinogenic factors, which has the characteristics of heterogeneity, immortalization, invasion, and metastasis. The tumor microenvironment, which is composed of immune cells and inflammatory cells, tumor-associated fibroblasts, micro-vessels, cytokines, and chemokines and is closely related to tumor occurrence, growth, metastasis, and recurrence. The tumor microenvironment is typically weakly acidic, with low oxygen levels and high reactive oxygen species (ROS) levels, and immunosup-

pression (Fig. 1). Enhanced aerobic glycolysis (*i.e.*, the Warburg effect) benefits tumor cell survival and invasion [42], and the large accumulation of lactic acid provides favorable conditions for the migration and immune escape of tumor cells [43,44]. A hypoxic microenvironment activates the hypoxia-inducible factor-1 (HIF-1) signaling pathway, which accelerates tumor growth, increases tumor invasiveness, promotes tumor metastasis, and leads to tumor drug resistance [45,46]. Almost all tumor cells have an imbalance in the intracellular redox system and the ROS levels in tumor cells are abnormally increased. Prolonged high levels of oxidative stress for a long time can induce DNA damage, protein modification and genomic instability, leading to potential carcinogenic mutations [47]. In addition, the immunosuppression of the microenvironment is closely related to tumor growth, invasion, and metastasis. The tumor-promoting M2 phenotype of tumor-associated macrophages assists cancer cell metastasis, angiogenesis, and proliferation via various anti-inflammatory mechanisms [48]. Moreover, the tumor microenvironment actively recruits regulatory T lymphocytes (Tregs), whose expansion and activation seem to respond to signals generated by tumors, thereby leading to tumor escape [49].

3. Magnesium alloy degradation and byproducts

Mg and its alloys are prone to corrosion. In the degradation process, Mg loses electrons and undergoes anodic reaction (Eq. (1)) while a large number of electrons undergo a cathodic reaction with H_2O (Eq. (2)). Subsequently, Mg^{2+} generated by the anodic reaction reacts with OH^- generated by the cathodic reaction to form the corrosion product $Mg(OH)_2$ (Eq. (3)). $Mg(OH)_2$ is unstable in aqueous solution, especially in the environment containing Cl^- . A high Cl^- concentration will accelerate the reaction of $Mg(OH)_2$, thereby promoting the corrosion of Mg, which produces high concentrations of Mg^{2+} and OH^- (Eq. (4)). The corrosion of these biomaterials mainly involves galvanic pitting, filamentous, and total corrosion, stress corrosion cracking, and corrosion fatigue (Fig. 2).



In galvanic corrosion, due to the low electrode potential of Mg, when Mg is in contact with other metals it generally serves as the anode for galvanic corrosion, while the cathode is a foreign metal directly in contact with the outside or a second phase or impurity phase inside the Mg alloy [50]. Macroscopically, the galvanic corrosion of the Mg alloy matrix and internal second phase is total corrosion. Metals with a low hydrogen overpotential form corrosive micro-batteries

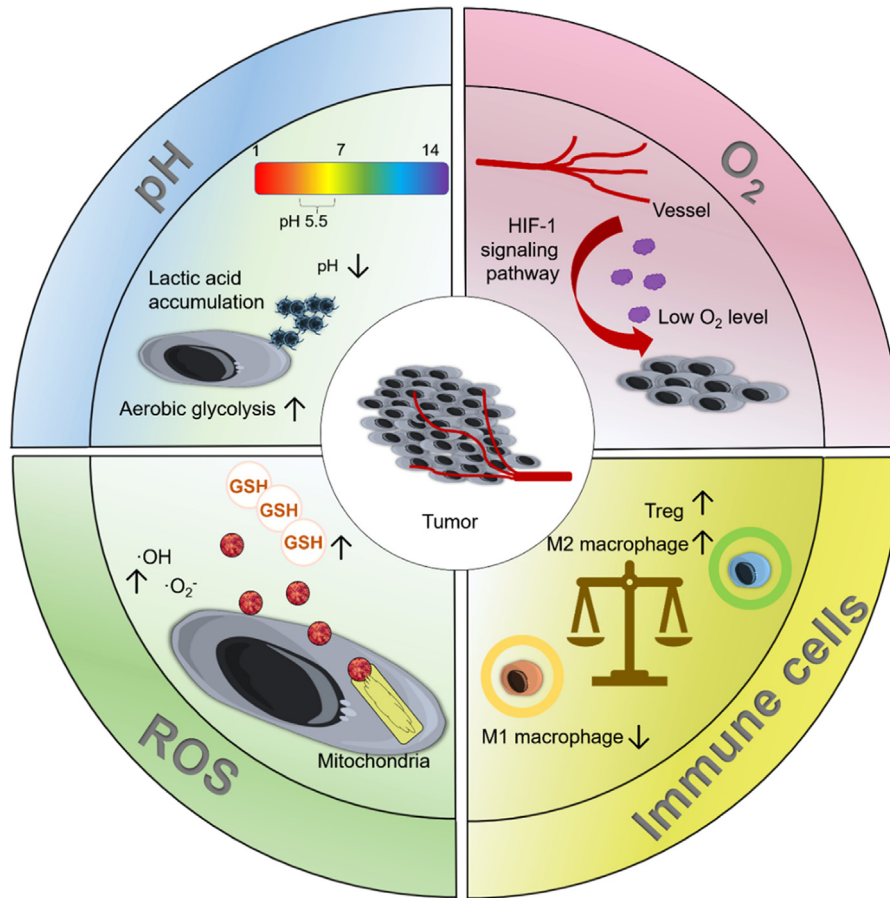


Fig. 1. Biological characteristics of tumors.

with Mg, resulting in marked galvanic corrosion of Mg alloys. However, metals with a higher hydrogen overpotential have less corrosion effects on Mg alloys [51]. The influence of the second phase on the corrosion of Mg alloys is well understood [52–54], but the phenomenon of cathode activation in the process of the corrosion of Mg alloys requires further exploration to determine whether it is the effect of impurities or a secondary phase, or a combination of both (Fig. 2A).

In pitting and filamentous corrosion, as Mg is a self-passivating metal, when Mg and Mg alloys are exposed to a non-oxidizing medium such as Cl^- , the unstable oxide film on its surface is destroyed, forming pitting corrosion [55]; corrosion pits are seen on the surface after gradually deepening. Active corrosion batteries generally have a protective coating or anodized oxide layer, which causes filamentous corrosion when it moves through the metal surface [56] (Fig. 2B).

In stress corrosion cracking, Mg alloys crack when stress applied in an environment with corrosion does not reach half the yield strength [57]. This corrosion is usually attributed to one of two mechanisms: continuous crack propagation caused by anodic dissolution of the crack tip or discontinuous crack propagation caused by a series of mechanical fractures of the crack tip [58]; that is, stress corrosion cracking has dissolution and brittle fracture models (Fig. 2C).

In corrosion fatigue, the fatigue strength increases with decreasing grain size, while the opposite is true for resistance to fatigue crack propagation [59]. Corrosion fatigue cracks propagate in a trans-granular/inter-granular composite manner, and the same environment that accelerates stress corrosion crack propagation also accelerates corrosion fatigue crack propagation (Fig. 2D). For example, the fatigue strength or fatigue life is significantly reduced in NaCl solution [60]. In general, the corrosion mechanism of Mg and Mg alloys is roughly expressed by the above equation.

4. Application of magnesium alloys in tumor treatment

Pure Mg is regarded as a relatively safe material. However, the mechanical properties of pure Mg are not sufficiently strong and the degradation rate of Mg with impurities (iron, nickel, and copper) is particularly rapid, hindering its further application [10]. Regardless of proper processing, the strength of pure Mg is low; specifically, the yield tensile strengths are 21 MPa for as-cast Mg, 90–105 MPa for as-extruded Mg, and 115–140 MPa for as-rolled Mg [61]. To improve the mechanical properties and degradation properties of Mg-based alloys for antitumor treatment, various approaches including

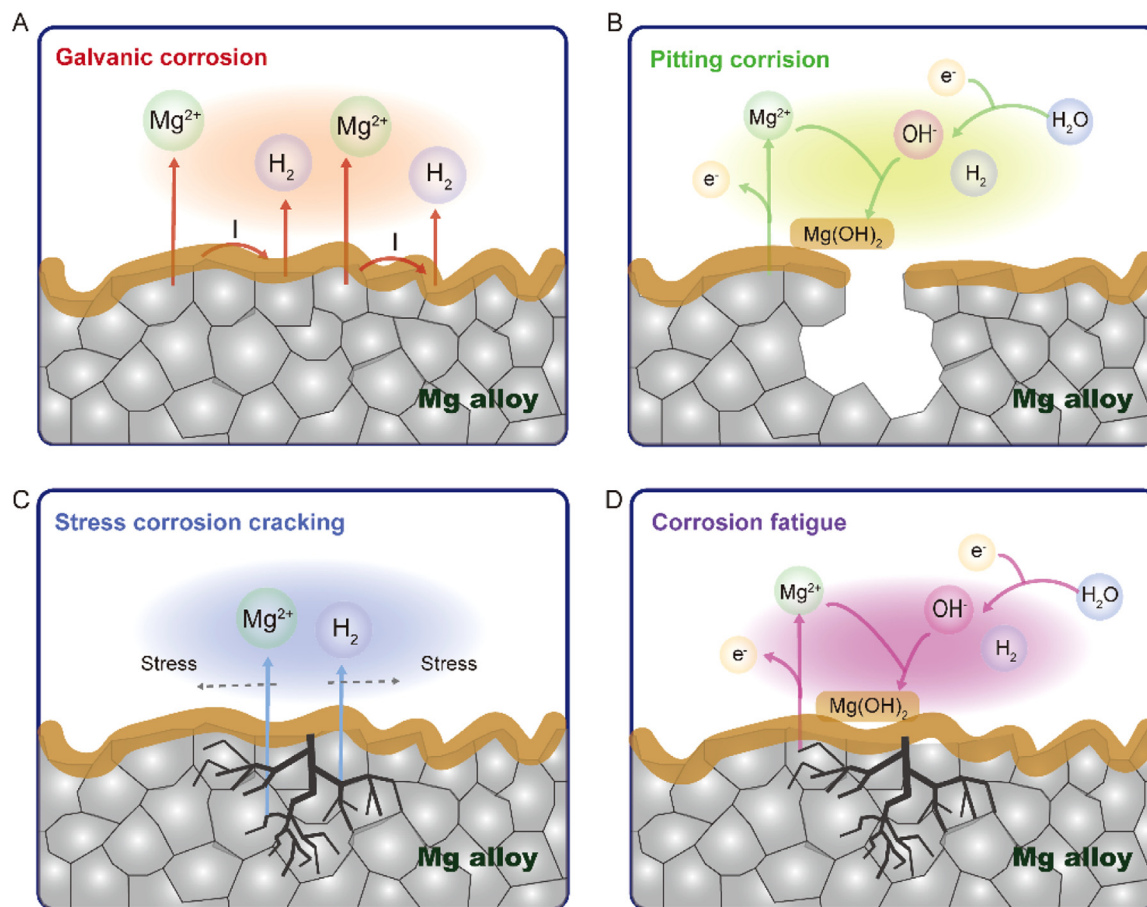


Fig. 2. The corrosion schematic diagrams of Mg alloys.

alloying and surface modification have been adopted, as shown in Table 1.

Alloying is one of the most effective ways to improve the corrosion resistance and mechanical strength of pure Mg. The alloying element Ca refines the microstructure of Mg through the formation of thermally stable intermetallic phases, improving strength and creep properties under high temperatures [10]. Wan et al. reported that the addition of an appropriate amount of Ca can effectively improve the flexural and compressive strength of pure Mg [62]. To further optimize the mechanical properties and degradation rate of Mg-Ca binary alloys, the essential elements Zn and Sr have also been introduced for improved alloy strength and ductility. Berglund et al. [63] reported that the slowest degradation of the Mg-1Ca-0.5Sr alloy was 1.5 mm/year in Hank's solution, but it remained able to maintain appropriate compressive strength (274 ± 4 MPa). On this basis, the addition of Zn can contribute to the formation of the eutectic phase and further reduce the alloy degradation rate. Wu et al. [22,64] reported the corrosion performance of a series of Mg-1Ca-0.5Sr-xZn ($x = 0, 2, 4, 6\%$) alloys in Hank's solution, where the addition of Zn significantly reduced the degradation rate of Mg-1Ca-0.5Sr in the initial stage. Additionally, Zn^{2+} and Mg^{2+} released from Mg-1Ca-0.5Sr-xZn significantly inhibited OS cell proliferation by altering the cell cycle and inducing cell apoptosis. Birblis et al. [65] found that the mechanical and degra-

ation properties of Mg alloys can be effectively improved by adjusting the ratio of REEs with different solubilities and heat treatments. Shuai et al. [21] reported that the compressive strength of Mg-6Zn-0.5Zr-xLa ($x = 0.5, 1.0, 1.5$ and 2.0 wt%) increased according to La content; the degradation rate decreased to 1.23 mm/year with an La content of 1.0 wt%. Upon the addition of La, the mitochondrial membrane potential decreased, whereas the ROS increased, revealing a high inhibition rate for OS cells.

Surface modification is another effective way to decrease the degradation rate and improve the biocompatibility of Mg alloys. Kannan et al. [20] electrophoretically deposited samarium on anodized AZ31 Mg alloy. Compared with the bare alloy, the corrosion potential of the samarium coating shifted in the positive direction, and the corrosion current density was significantly reduced. The Bode phase angle diagram showed that the phase angle value in the mid-frequency region was higher than the value of the bare alloy; this finding indicated that the coating prevented the solution from penetrating the alloy, suggesting that the Mg alloy with samarium coating had greater corrosion resistance. Additionally, samarium-coated Mg alloys showed excellent performance with respect to anti-bone tumor relapse and metastasis effects.

Through a series of modification, Mg alloys gain better mechanical properties and degradation rates, which laid a good foundation for its anti-tumor application, including but

Table 1
Summary of the mechanical properties, *in vitro* biodegradability of the representative Mg alloys for antitumor applications.

Material	Working history	Mechanical properties	<i>In vitro</i> corrosion		Reference
			Corrosion medium	Degradation rate (mm/year)	
Mg wire (99.98%)	Casting	–	SBF solution	~ 1	Shuang Qiao [36]
Mg wire (99.98%)	Extruded, drawn	Ultimate tensile strength: 195.1 MPa Elongation: 17.0%	SBF solution	~ 1	Rui Zan [38]
As-cast Mg wire (99.95%)	Extruded	Ultimate tensile strength: 175 ± 5.6 MPa Elongation: 4.8 ± 0.5%	SBF solution	~ 1	Rui Zan [31]
Mg-1Ca-0.5Sr-xZn (x = 0, 2, 4, 6 wt%)	Extruded	–	Hank's solution	The addition of Zn significantly decreased the MDR of Mg-1Ca-0.5Sr.	Yuanhao Wu [22,64]
Mg-xLi-Zn (x = 3, 6, 9%)	Extruded	With the increase of Li content, the YS and tensile strength of alloy decreased	SBF solution	–	Jingan Li [25]
Mg-2.0%Ag	Extruded with ECAP	Ultimate tensile strength: 182 ± 7 MPa Tensile yield strength: 53 ± 5 Mpa Elongation: 23.7 ± 0.6%	DMEM + 10% FBS + 100 mg/mL penicillin-streptomycin + 2 mM glutamine	0.96 ± 0.14 (incubation 2 d) 1.47 ± 1.47 (incubation 7 d)	Yuri Estrin [88]
Mg-4.0%Ag	Extruded with ECAP	Ultimate tensile strength: 204 ± 5 MPa Tensile yield strength: 42 ± 5 MPa Elongation: 27.3 ± 2.1%	DMEM + 10% FBS + 100 mg/mL penicillin-streptomycin + 2 mM glutamine	2.31 ± 0.33 (incubation 2 d) 1.43 ± 0.35 (incubation 7 d)	Yuri Estrin [88]
Mg-6%Ag	Extruded	–	DMEM + 10% FBS + 100 mg/mL penicillin-streptomycin + 2 mM glutamine	~ 0.75 (incubation 1 d) ~0.35 (incubation 3 d) ~0.25 (incubation 7 d)	Philipp Globig [117]
Mg-6.0%Ag	Extruded with ECAP	–	RPMI-1640 + 10% FBS + 1% penicillin-streptomycin + 4 mM/L glutamine	4.04 ± 0.48	Natalia Anisimova [86]

(continued on next page)

Table 1 (continued)

Material	Working history	Mechanical properties	<i>In vitro</i> corrosion		Reference
			Corrosion medium	Degradation rate (mm/year)	
Mg-6%Nd-2%Y-0.5%Zr	Rapid solidification + Extrusion	α - Mg matrix hardness: 94.3 ± 2.6 HV Mg-oxide hardness: 277.3 ± 21.2 HV	0.9% NaCl saturated with Mg(OH) ₂ solution	–	O. Hakimi [118,119]
Mg-6Zn-0.5Zr-xLa (x = 0.5, 1.0, 1.5 and 2.0 wt%)	Selective laser melting	Compressive strength: 151.2 ± 4.3 MPa (0.5 La), 169.4 ± 5.1 MPa (1.0 La), 163.7 ± 4.5 MPa (1.5 La), and 158.8 ± 5.0 MPa (2.0 La) Hardness: 104.9 ± 5.2 HV (2.0 La)	SBF solution	1.23	Cijun Shuai [21]
Mg-3.56%Y-2.20%Nd-0.47%Zr	Extruded with ECAP	–	RPMI-1640 + 10% FBS + 100 mg/mL penicillin-streptomycin + 2 mM glutamine	1.57 ± 0.19	Natalia Anisimova [37]
Mg-10.0%Gd	Extruded with ECAP	–	RPMI-1640 + 10% FBS + 1% penicillin-streptomycin + 4 mM/L glutamine	2.77 ± 0.46	Natalia Anisimova [86]
Mg-Zn-Y-Nd	Extruded	Micro hardness: 54.3 ± 2.5 HV	Hank's solution	0.25 ± 0.10	Shuo Wang [16]
Samarium-coated Mg alloy	Extruded	–	SBF solution	~ 0.4	Saranya Kannan [20]
Fe ²⁺ -coated Mg alloy	Extruded	–	PBS solution/0.9 wt% NaCl	Fe ²⁺ coating performed better corrosion resistance	Dongdong Zhang [120]

SBF solution: Simulated body fluid solution; PBS: phosphate-buffered saline; FBS: fetal bovine serum; DMEM: Dulbecco's Modified Eagle's Medium; ECAP: Equal-channel angular pressing; MDR: mean degradation rate.

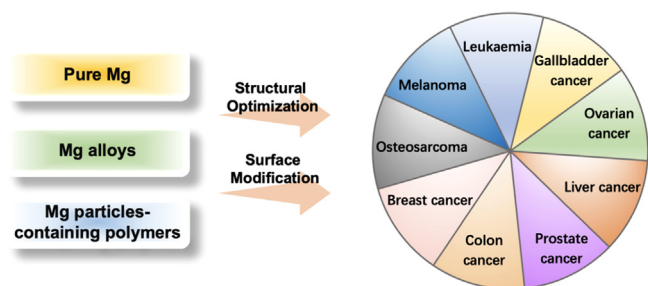


Fig. 3. Magnesium alloys in antitumor applications.

not limited to osteosarcoma (OS) [19–31], breast [8,32–35], ovarian [36], prostate [37], colon [38,39], gallbladder [40], liver [41], and other cancers (Fig. 3).

4.1. Bone tumors

As a primary malignant bone tumor originating from bone mesenchymal cells, OS is common in children and adolescents, with high malignancy and rapid progression [66]. The current treatment of OS is radical surgery combined with chemotherapy, and the extensive bone tissue loss and unavoidable residual tumor cells caused by surgery have a great impact on the patients' prognosis and quality of life [67]. Hence, it is important to develop novel biomaterials with dual functionalities, including the efficient elimination of residual cancer cells to prevent tumor recurrence and the ability to promote bone regeneration to repair large surgical defects.

Mg alloys can not only inhibit tumor cells growth but also promote new bone formation in the bone defect after tumor resection, showing the great potential of the multifunctional effect of Mg alloys in anti-bone tumor applications [19,28,38]. Table 2 summarize the anti-bone cancer effects of Mg alloys in the literature, and Fig. 4 displays some representative experimental results.

Pure Mg wires activate the transport of zinc finger protein Snail1 from the cytoplasm to the nucleus by releasing Mg^{2+} , thereby inducing OS cell apoptosis and inhibiting OS cell proliferation. Furthermore, the hydroxide gas produced by Mg wires eliminates excessive intracellular ROS, inhibiting bone tumor cell growth [31]. Milenin et al. [29] utilized MgCa0.7 alloy for the treatment of OS cells, they found that it could inhibit SaOS-2 cells. Additionally, the antitumor effect and degradation of Mg alloys can be improved by modifying the surface of the Mg alloy and loading active ingredients. Li et al. [26] developed a novel approach using a bisphosphonate (BP)-loaded microarc oxidation coated Mg-strontium alloy pellet to inhibit OS. The BP-coated Mg pellets destroyed tumors and prevented neoplasm recurrence by inducing apoptosis, necrosis, and synergistic effects of Mg degradation. Shao et al. [68] and Zhang et al. [30] fabricated a layered double hydroxide on Mg alloys surface, which enhanced its antitumor effects.

The porous structure of Mg alloys allows for cell infiltration and promotes the attachment and growth of bone-forming cells [30]. As the alloy degrades, it releases Mg ions, which

have antitumor effects on OS cells. This dual action of providing structural support while exerting anticancer properties makes Mg alloys a promising option for bone cancer therapy.

Besides the direct effect on tumor cells, Mg particle solutions absorb light throughout the entire ultraviolet–visible–near infrared region (300–900 nm), and have potential as photothermal agents (PTAs) [28]. Photothermal therapy (PTT) is an established therapeutic strategy for cancer that harvests light energy and converts it into heat to raise the temperature of the surrounding environment and trigger tumor cell death [69,70]. Compared with traditional therapies, PTT has the advantages of high accuracy, noninvasiveness, and precise spatiotemporal selectivity [71–74]. Mg alloys have been explored as PTAs [28,41]. Conventional PTAs mainly use metal elements with slow degradation rates such as copper (Cu) and gold. To achieve better photothermal conductivity, a high PTA concentration may produce side effects, such as high concentrations of Cu^{2+} that significantly inhibit cell proliferation [75]. Since Mg particles can be used directly as PTA without loading particles, the above drawback can be overcome, and good photothermal conversion properties and positive effects on surrounding healthy tissues can be achieved simultaneously. Long et al. [28] reported the synthesis of dual-functional poly(lactide-co-glycolide)/Mg scaffolds with excellent photothermal conversion ability. Their study suggests that Mg alloys combined with PTT are potential biomaterials for OS applications. Table 3 summarizes the PTT conditions of Mg alloys used for antitumor applications from representative publications.

Additionally, the implanted bioactive scaffolds can stimulate the osteogenic differentiation capacity of bone marrow stromal cells (BMSCs) via Mg^{2+} , thereby promoting the production of new bone in areas with bone deficiencies [28,76]. Typically, bioactive scaffolds have porous structures, which facilitate nutrient transport and ion exchange, enabling the gradual release of Mg^{2+} during degradation, thereby realizing truly dual-functional bioactive scaffolds [77]. In addition to antitumor effects, Mg alloys can promote bone regeneration *in vivo* and *in vitro* [12,28,30,68,78–80]. *In vitro* osteogenic development studies have examined rat BMSCs [12], rabbit BMSCs [78,79], MC3T3-E1 cells [28,80], human umbilical vein endothelial cells (HUVECs) [80], and C3H10T1/2 cells [30,68]. The test groups performed significantly better based on alkaline phosphatase activity, alizarin red S staining, and the expression levels of osteogenic-related genes including runt-related transcription factor 2 (Runx2), bone sialoprotein (BSP), osteopontin (OPN), and osteocalcin (OCN).

4.2. Breast cancer

Breast cancer is the most diagnosed cancer among women worldwide, and one of the leading causes of cancer-related death in women [81]. Current treatment for breast cancer typically involves a combination of surgery, chemotherapy, radiation therapy, and targeted therapy. These treatments are tailored to the specific characteristics of the tumor and aim to remove or shrink the tumor, eliminate cancer cells, and

Table 2
Summary of the *in vitro*, *in vivo* studies and active ingredients of the Mg alloys for anti bone cancer applications.

Materials	<i>In vitro</i> studies		<i>In vivo</i> studies		Active ingredients for antitumor effects	Ref.
	Cell type	Results	Animal model (cell type)	Results		
Mg-1Ca-0.5Sr-xZn (x = 0, 2, 4, 6 wt%) Control: Ti-6Al-4 V alloy	U2OS cell	<p>a) MTT assay: With the increase of Zn content in the alloys, the ability of Mg alloy to inhibit tumor cells was significantly elevated.</p> <p>b) Cell invasion test: Mg-1Ca-0.5Sr-6Zn alloy process better effect on suppressing the invasion of U2OS cells <i>in vitro</i> than other groups.</p> <p>c) Cell cycle distribution analysis: The Mg alloys extracts inhibited U2OS cell proliferation via inducing G2/M phase arrest and G0/G1 phase reduction.</p> <p>d) Apoptotic potential test: The Mg alloys showed an apoptosis effect to the U2OS cells, especially for the Mg-1Ca-0.5Sr-6Zn.</p>	–	–	Transportation of Zn ²⁺ into cell and higher intracellular Zn ²⁺ concentration induced dysfunction of mitochondrion. ROS accumulated in mitochondrion and regulated the protein expression levels. And the upregulation of Bac and p53 and down regulation of Bcl-2 lead the cell apoptosis.	Yuanhao Wu, 2016 [22]
ZK60: Mg-6Zn-0.5Zr ZK60-xLa (x = 0.5, 1.0, 1.5 and 2.0 wt%)	U2OS cell: for antitumor effect HEK 293 cell: for cytotoxicity effect	<p>a) CCK-8 assay: The cell viability of the U2OS cells cultured in ZK60, ZK60–0.5La, ZK60–1.0La, ZK60–1.5La, and ZK60–2.0La extracts for 5 d were 94.2%, 50.8%, 38.1%, 31.4%, and 25.2%, respectively. And ZK60-La showed no toxicity to HEK 293 cells.</p> <p>b) Live/Dead staining: To U2OS cells, dead cells gradually increased and live cells decreased in ZK60-La extracts for 5 d with La content increasing. And ZK60-La showed no toxicity to HEK 293 cells.</p> <p>c) Detection of changes in mitochondrial membrane potential: The level of MMP decreased in the U2OS cells with the La content increasing.</p> <p>d) ROS test: The ROS level increased in the U2OS cells with the La content increasing.</p>	–	–	The La ³⁺ could replace the Ca ²⁺ binding to the binding sites on the mitochondrial permeability transition pore (mPTP). The decrease of mitochondrial membrane potential and the generation of ROS lead the cell apoptosis.	Cijun Shuai, 2018 [21]

(continued on next page)

Table 2 (continued)

Materials	<i>In vitro</i> studies		<i>In vivo</i> studies		Active ingredients for antitumor effects	Ref.
	Cell type	Results	Animal model (cell type)	Results		
Ex-Mg-1Ag-1Y: as extruded Mg-1Ag-1Y (1 wt% Ag, 1 wt% Y)	–	–	Bone tumor bearing model of nude mice (MG63 cell)	<p>a) The tumor growth curves: Relative to the Ti alloy group, the Mg alloy and pure Mg group displayed a more effective ability to inhibit the tumors around the metals and impede the corrosion processes in the gross specimens.</p> <p>b) Examination of pulmonary metastasis: After 5 weeks post-operation, several nodes were found on the pulmonary surface of the Ti alloy group, while it was rare to find them in the Mg alloy and pure Mg animal groups.</p>	<p>a) Changed the extracellular acidosis microenvironment</p> <p>b) Elevated the Mg concentration</p> <p>c) Suppressed C-X-C chemokine receptor type 4 (CXCR4) levels and increased prostacyclin (PGI2) synthesis</p>	Yilong Dai, 2019 [19]
Samarium-coated Mg alloy	MG63 cell: for antitumor effect MSCs: for cytotoxicity effect	<p>a) MTT assay: The anticancer activity was good at 50 and 100% extract concentration. The inhibition activity was proximate 35% in the 50% extract concentration. An exceptional anticancer activity of 87 and 96% was observed for 100% extract concentration at 48 and 72 h, respectively. The cell viability percentage of MSCs is ~72% in contrast to the blank control.</p>	–	–	The permeability of the cell membrane was influenced by the lanthanides as their cationic size is like calcium ions.	Saranya Kannan, 2020 [20]

(continued on next page)

Table 2 (continued)

Materials	<i>In vitro</i> studies		<i>In vivo</i> studies		Active ingredients for antitumor effects	Ref.
	Cell type	Results	Animal model (cell type)	Results		
PLGA/Mg composite scaffolds: P5M with 5 wt% Mg P10M with 10 wt% Mg P15M with 15 wt% Mg	MC3T3-E1 cell: for cytotoxicity effect Saos-2 cell: for antitumor effect	<p>a) CCK-8 assay: Saos-2 cell proliferation was decreased by PLGA/Mg scaffolds while MC3T3-E1 cell proliferation was increased.</p> <p>b) Annexin V/PI staining: Laser irradiation significantly increased the percentage of apoptotic cells in Saos-2 cells (94.6% versus 42.4%), whereas no significant apoptosis was observed in MC3T3-E1 cells.</p> <p>c) Western blot assay: The expression of Bcl-2 decreased when cultured on P10M scaffolds.</p>	Bone tumor bearing model of nude mice (Saos-2 cell)	<p>a) Three-dimensional fluorescence imaging system: The intrinsic antitumor properties of P10M scaffold can produce significant and effective inhibition of tumor recurrence.</p> <p>b) The tumor growth curves: No tumor recurrence was observed in the P10M + NIR group, and the mice didn't show significant weight loss.</p> <p>c) Immunohistochemistry staining: Osteocalcin, Ki67 and P53 were barely visible in the P10M + NIR group; significant Ki67 and P53 were observed in the P10M group, indicating that P10M has an inhibitory effect in inducing apoptosis.</p>	<p>a) PTT effect</p> <p>b) Tumor microenvironment modulation effect</p>	Jing Long, 2020 [28]
As-cast Mg wires	MG63 and U2OS cell: for antitumor effect C28/I2 cell: for cytotoxicity effect	<p>a) CCK-8 assay: Mg wires inhibit the viability of OS tumor cells.</p> <p>b) Apoptosis analysis: The apoptosis rate of the OS cells was increased with the concentration of Mg²⁺.</p> <p>c) RT-qPCR and Western Blot assay: Mg²⁺ promotes nuclear import and phosphorylation of Snail1 protein. The expressions of miRNA-181c-5p and miRNA-181d-5p in OS cells were down-regulated with increasing Mg²⁺.</p>	Bone tumor bearing model of nude mice (MG63 cell)	<p>a) The tumor growth curves: Compared with the mice without implantation of Mg wires, the Mg wires could significantly inhibit the growth of subcutaneous tumors, while the rapid growth of tumors was observed in the miRNA-181c/d-5p overexpressed group.</p> <p>b) Histopathological analyses: A lower density of tumor cell nuclei was observed in the H&E staining, and the cell shape is relatively homogeneous in the Mg group. Ki67-positive (brown) tumor cells declined quickly after treatment with Mg wires.</p>	Mg ²⁺ could effectively suppress the expression of miRNA-181c/d-5p, promotes the death of OS cells by increasing the NLK and TIMP3 expressions through the miRNA-regulated post-transcription.	Rui Zan, 2021 [31]

(continued on next page)

Table 2 (continued)

Materials	<i>In vitro</i> studies		<i>In vivo</i> studies		Active ingredients for antitumor effects	Ref.
	Cell type	Results	Animal model (cell type)	Results		
BP coated Mg: bisphosphonate coated magnesium-strontium alloy pellet MAO coated Mg: microarc oxidation coated magnesium-strontium alloy pellet	UMR-106 cell	<ul style="list-style-type: none"> a) CCK-8 assay: The cell viability rate was all less than 20% in BP coated Mg group. b) Live/Dead staining: More than 80% of the tumor cells in the BP coated Mg group are dead. c) Apoptosis analysis: OS cells in the BP coated Mg group were in late apoptosis and necrosis. d) Cell cycle analysis.: The BP coated Mg pellet extracts leads to a significant decrease in the Sub G1 fraction and an increase in the G2 /M fraction compared with other treatments. e) Cell migration analysis: BP coating inhibit the invasive ability and further metastasis of OS cells. 	Bone tumor bearing model of nude mice (UMR-106 cell)	<ul style="list-style-type: none"> a) The tumor growth curves: BP coating inhibited the tumor growth. b) Histopathological analysis: For the BP coated Mg group, severe damage to the tumor tissues and irreversible necrosis were identified around the pellets. Ki-67 and p65 were highly expressed around the pellets in Bare Mg and MAO coated Mg groups. While for the BP coated Mg group, the expression of Ki-67 and p65 was negative. 	The BP coated Mg pellets could significantly suppress the mevalonate pathway at the molecular biology level in OS cells compared to other Mg pellets.	Mei Li, 2021 [26]
MgCa0.7 alloy	SaOS-2 cell: for antitumor effect hPDL cell: for cytotoxicity effect	<ul style="list-style-type: none"> a) MTT assay: The material after extrusion exhibited the largest average absolute difference in the viability of healthy and cancer cells among the studied extract ratios, with a value of 23.3%. Additionally, after hot drawing at the maximum temperature, the viability difference was observed to be 21.2%. 	–	–	Mg alloys could inhibit tumor cell growth without harming healthy cells.	Andrij Milenin, 2021 [29]

(continued on next page)

Table 2 (continued)

Materials	<i>In vitro</i> studies		<i>In vivo</i> studies		Active ingredients for antitumor effects	Ref.
	Cell type	Results	Animal model (cell type)	Results		
Mg-xLi-Zn alloys (x = 3, 6, 9)	MG-63 cell: for antitumor effect MC3T3-E1 cell: for cytotoxicity effect	a) MTT assay: All the Mg-xLi-Zn alloys exhibited potent inhibitory effects on osteosarcoma. The viability of MC3T3 cells in all Mg-xLi-Zn alloy groups remained above 80%. Specifically, the Mg-3Li-Zn and Mg-6Li-Zn groups promoted the proliferation of MC3T3 cells at certain concentrations of degradation products.	–	–	Mg alloys could inhibit tumor cell growth while promoting the proliferation of MC3T3 cells.	Jingan Li, 2021 [25]
GO-1#, GO-2#, GO-3#: graphene oxide coated AZ31 Mg alloy rGO-1#, rGO-2#, rGO-3#: reduced graphene oxide coated AZ31 Mg alloy	MG63 cell	a) Cell viability test: Only 40% of cells were alive when the rGO-2# samples were under irradiation. For comparison, cells cultured with AZ31 (with or without irradiation) and rGO-2# (without irradiation) showed no significant difference with that cultured on the control group (Blank).	–	–	PTT effect	Lidan Liu, 2022 [27]
LDH-Mn: Black Mn-containing LDH film-modified Mg alloy; PEO/LDH: Plasma electrolytic oxidation/LDH coating sample; LDH-Mn1/2/3: different MnCl ₂ aqueous solution immersing time (3/6/9 h respectively)	MC3T3-E1 cell: for cytotoxicity effect SaOS-2 cell and UMR106 cell: for antitumor effect	a) Fluorescein isothiocyanate (FITC) - phalloidin and 4',6-diamidino-2-phenylindole (DAPI) staining: Under NIR laser irradiation, the tumor cells on LDH-Mn3 were entirely destroyed. b) AlamarBlue™ assay: At each of the three detection time points, there were noticeably more cells on the LDH-Mn2 and LDH-Mn3 sheets than on the other two groups. c) Live/dead staining: Due to their improved anti-corrosion abilities, the LDH-Mn2 and LDH-Mn3 groups showed more living cells. d) Protein adsorption: Compared to the other samples, the LDH-Mn3 sample had a much higher ability for protein adsorption. e) Hemolysis assay: The PEO/LDH sample's hemolysis rate value was significantly higher than the permitted level of 5%.	Bone tumor bearing model of nude mice (UMR106 tumor cells)	a) The tumor growth curves: With NIR radiation, the tumor's development was significantly reduced. b) The pathological analyses, including H&E, TUNEL, and Ki67: Fewer tumor nuclei were observed in the LDH-Mn3 + NIR group tumor tissues, while significant apoptosis and restricted proliferation were seen compared to other groups.	a) PTT effect b) Nanocatalytic Fenton-like performance	Dongdong Zhang, 2022 [30]

(continued on next page)

Table 2 (continued)

Materials	<i>In vitro</i> studies		<i>In vivo</i> studies		Active ingredients for antitumor effects	Ref.
	Cell type	Results	Animal model (cell type)	Results		
Mg (pure: 99.95 wt%) Mg–6Ag (Mg with 6 wt% Ag)	RF Fibroblasts: for cytotoxicity effect SaoS-eGFP cells: for antitumor effect	a) Immunofluorescence: The number of cancer cells on Mg and Mg–6Ag was significantly lower. b) Ki-67 and p38 immunostaining: Mg-based materials inhibit Saos-eGFP cell proliferation. c) ELISA: elevated IL-8 secretion from the coculture on Mg-based materials.	–	–	The Mg degradation dependent pH increased.	Philipp Globig, 2022 [24]
Mg (pure: 99.95 wt%) Mg–6Ag (Mg with 6 wt% Ag)	Saos-eGFP cells and RF Fibroblasts: for monitor cell migration and cell invasion HUVEC: for monitor cancer-induced angiogenesis	a) Microscopic images: Mg alloys reduced cell migration and invasion; Mg exposition affected endothelial cell proliferation, migration and tube formation. b) Enzyme-linked immunosorbent assay (ELISA): Mg alloys increased MMP-2, MMP-9 release. c) VEGF concentration: Mg alloys reduced angiogenesis initiation.	–	–	Mg alloys inhibited cell migration and invasion and can potentially reduce the cancer-induced angiogenesis at an early step.	Philipp Globig, 2023 [23]
PEO: plasma electrolytic oxidation AZ31 Mg alloy LDH: Fe@PEO + hydro-thermal treatment in water FeOOH: LDH + Fe ²⁺ TR1/2-FeOOH: thermal treatment in H ₂ /Ar for 90/180 min	MC3T3-E1 cell: for cytotoxicity effect SaOS-2 cell: for antitumor effect	a) Hemolysis Rate test: after the coating protection, the hemolysis rate was reduced to <5%. b) Alamar Blue assay and Live/Dead staining: Prepared Fe-based coatings possess excellent biocompatibility. And reduced FeOOH coatings exhibited excellent NIR-induced anti-tumor ability.	Bone tumor bearing model of nude mice (UMR106 tumor cells)	a) The tumor growth curves: The tumor's development of TR2-FeOOH-NIR group was significantly reduced. b) H&E, Ki67, and TUNEL staining: With NIR radiation, the tumor's development of TR2-FeOOH group was significantly reduced.	a) The coating enhanced the corrosion resistance and biocompatibility of bare Mg alloys. b) PTT effect c) CDT effect	Dongdong Zhang, 2023 [120]

MSCs: Mesenchymal stem cells; LDH: layered double hydroxide; CCK-8: Cell Counting Kit-8; PTT: photothermal therapy; ROS: Reactive Oxygen Species; TUNEL: TdT-mediated dUTP nick end labeling; EPD: electrophoresis deposited; MMP: matrix metalloproteinases; VEGF: vascular endothelial growth factor; CDT: chemodynamic therapy.

Table 3
Summary of the Photothermal therapy conditions of the Mg alloys for antitumor applications.

Material	Photothermal agent	Wavelength (nm)	<i>In vitro</i> studies			<i>In vivo</i> studies			Ref.
			Power density (W/cm ²)	Irradiation time (min)	Highest temperature (°C)	Power density (W/cm ²)	Irradiation time (min)	Highest temperature (°C)	
Chit-Mg MPs	Mg mi-crostructures	808	13.0	3.0	50.0	1.0 / 3.0	0.5 / 2.0	-	Robert. C. Martin, 2016 [41]
Mg@PLGA microspheres/nanospheres	Mg mi-cro/nanostructures	808	0.7	4.0 / 10.0	40.0 / 55.0	0.7	10.0	-	Weixiao Zhou, 2020 [35]
PLGA/Mg composite scaffolds: P5M with 5 wt% Mg P10M with 10 wt% Mg P15M with 15 wt% Mg	Mg nanostructures	808	1.0	5.0	65.0	1.0	5.0	57.0 ± 6.7	Jing Long, 2020 [28]
LMM@BSA: Mg-Mn-Al alloy-MOS ₂ -bovine serum albumin LMM@BSA/Ce6: Mg-Mn-Al alloy-MOS ₂ -bovine serum albumin-chlorin e6	MOS ₂ nanostructures Ce6	808	1.0	5.0	ΔT=44	1.0	5.0	ΔT=16.0 (injected with 20 μL) ΔT=33.0 (injected with 200 μL) ΔT=14.0	Jiayan Zhao, 2021[39]
LDH-Mn: Black Mn-containing LDH film-modified Mg alloy; PEO/LDH: Plasma electrolytic oxidation/LDH coating sample; LDH-Mn1/2/3: 1/2/3 represented different MnCl ₂ aqueous solution immersing time (3/6/9 h respectively)	Mn nanostructures	808	0.8	10.0	LDH-Mn1: 52.0 LDH-Mn2: 55.0 LDH-Mn3: 57.0	1.0	5.0		Dongdong Zhang, 2022 [30]
PEO: plasma electrolytic oxidation AZ31 Mg alloy LDH: Fe@PEO + hydro-thermal treatment in water FeOOH: LDH + Fe ²⁺ TR1/2-FeOOH: thermal treatment in H ₂ /Ar for 90/180 min	Fe ²⁺	808	1.0	10.0	PEO: ~ 42.0 LDH: ~ 45.0 FeOOH: ~ 47.5 TR1-FeOOH: ~50.0 TR2-FeOOH: ~52.5	1.0	10.0	FeOOH: ~50.0 TR2-FeOOH: ~55.0	Dongdong Zhang, 2023 [120]

LDH: layered double hydroxide.

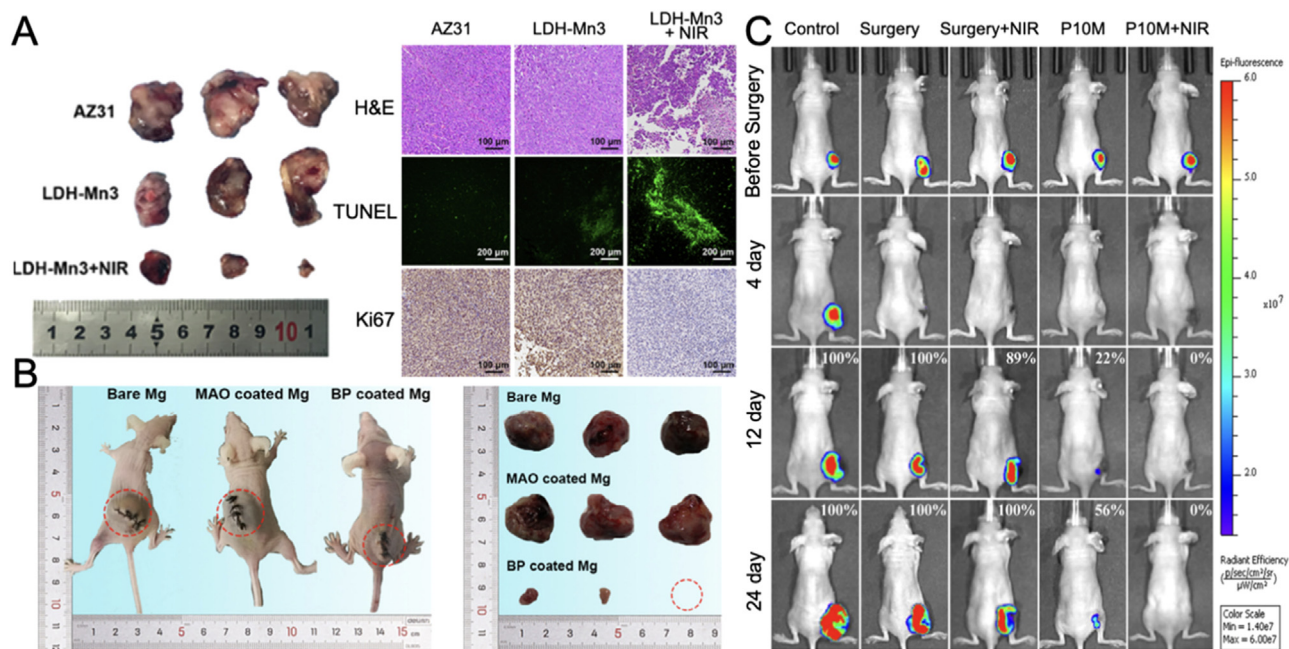


Fig. 4. Representative antitumor effect of Mg alloys for bone cancer: A. Photographs, H&E, TUNEL, and Ki67 staining of tumor tissue after nude mice treated with AZ31, LDH-Mn3, LDH-Mn3+NIR, respectively. (Reproduced with permissions from Ref. [30]) B. Representative photos of tumor-bearing nude mice and tumor tissues collected from mice treated with different Mg pellets at day 28. (Reproduced with permissions from Ref. [26]) C. *In vivo* images of tumor-bearing mice right before surgical removal of the solid tumors and after accepting different treatments for 4, 12 and 24 days. (Control: mice without implantation; Surgery: mice with PLGA scaffolds implantation; P10M: PLGA/Mg composite scaffolds with 10 wt% Mg). Reproduced with permissions from Ref. [28]) (LDH: layered double hydroxide; NIR: near-infrared light; MAO: microarc oxidation; BP: bisphosphonate).

prevent recurrence [82]. Advances in personalized medicine and targeted therapies have improved treatment outcomes and patient survival. Nevertheless, ongoing research and clinical trials are focused on developing novel treatment approaches to enhance the effectiveness and minimize side effects of breast cancer therapy. In particular, the treatment of triple-negative breast cancer remains a major challenge due to its greater degree of malignancy and the lack of genetic targets [83]. The chemotherapeutic agents currently used are mainly injected via artificial blood vessels, and have bioavailability issues; thus, local drug precision delivery systems and local tumor ablation have been introduced for breast cancer treatment. Porous drug-loadable Mg alloys and the tumor-suppressive effect of the Mg alloy degradation product H_2 have increased interest in Mg alloys for breast cancer treatment. Fig. 5 and Table 4 summarize the literature on the anti-breast cancer effects of Mg alloys.

Mg alloys with porous structures can be engineered, allowing for the controlled release of therapeutic agents. Liu et al. [32] invented MgNF@PEG/PMMVP [pH-sensitive polyethylene glycol-b-(poly(methyl methacrylate)-co-poly(4-vinylpyridine) (PEG-bPMMVP) coated with Mg nanoflowers], which can be implanted near a tumor and release Mg^{2+} . As the Mg degrades over time, Mg^{2+} directly targets the cancer cells while minimizing damage to healthy tissues. Mg alloy implants can be placed strategically near a tumor, providing the sustained controlled release of therapeutic agents directly to the affected area. This targeted drug delivery approach holds promise for enhancing the effec-

tiveness of chemotherapy, while minimizing systemic side effects.

Recent reports have highlighted the therapeutic potential of H_2 in free radical-related breast cancer. Given that Mg alloys release H_2 during their biodegradation, it is reasonable to consider Mg alloys a promising material with therapeutic properties for inhibiting breast cancer [8,84]. Recently, Liu et al. [32] reported pH-sensitive polymer-coated Mg nanoflowers for breast cancer treatment. In the tumor microenvironment, the continuous generation of H_2 was facilitated by the disassembly of the polymeric shell triggered by the acidic conditions. This disassembly allowed Mg to react with water, resulting in the production of H_2 bubbles, which induce transient cavitation and mechanical rupture of lysosomes. They also disrupt cellular energy metabolism, while simultaneously inducing high levels of oxidative stress. The combined effects of these processes ultimately lead to cancer cell death.

4.3. Other tumor types

While the applications mentioned above highlight specific tumor types, the potential use of Mg alloys in cancer treatment is not limited to these cases. Further research is exploring the efficacy of Mg alloys in other malignancies, including but not limited to prostate [37,86], colorectal [38,39,85], liver [41], ovarian [36], esophageal [16], and gallbladder [40] cancers, as well as melanoma [37,87], leukemia [88], and cholangiocarcinoma [89]. Fig. 6 provides representative *in*

Table 4
Summary of the *in vitro*, *in vivo* studies and active ingredients of the Mg alloys for anti breast cancer applications.

Materials	<i>In vitro</i> studies		<i>In vivo</i> studies		Active ingredients for antitumor effects	Ref.
	Cell type	Results	Animal model (cell type)	Results		
P-Mg: pure Mg AO-HT-Mg: pure Mg coating with MgO	MRMT-1 cell	<p>a) MTT assay: The OD values of cells on both P-Mg and AO-HT-Mg were significantly lower compared to the control (well without material) all the time and the cells on AO-HT-Mg proliferated faster than those on P-Mg metal.</p> <p>b) CLSM analysis: Cells cultured on the surface of AO-HT-Mg had better proliferation and extending than those on P-Mg.</p> <p>c) ROS assay: The order of the free radicals in the cells: AO-HT-Mg < P-Mg < control.</p>	Breast tumor bearing model of nude mice (4T1/Luc cell)	<p>a) The tumor growth curves: The tumor growth rate of the control group is significantly larger compared to both groups implanted with P-Mg or AO-HT-Mg. Before 26 days, the tumor growth rate of P-Mg group was slower than that of AO-HT-Mg group; after 26 days, the tumor growth rate of P-Mg group was significantly larger than that of AO-HT-Mg group.</p> <p>b) <i>In vivo</i> imaging analysis: Both P-Mg and AO-HT-Mg could inhibit the tumor growth.</p> <p>c) Malondialdehyde evaluation: The MDA levels in different groups of animals had an order of P-Mg < AO-HT-Mg < Blank (without 4T1/Luc cell, Mg implant) < Control (with 4T1/Luc cell, without Mg implant).</p> <p>d) Histological evaluation: Both P-Mg and AO-HT-Mg could promote cell apoptosis and necrosis within tumors and reduce the rate of tumor progression, and P-Mg had a higher ability compared to AO-HT-Mg.</p>	<p>a) Inhibited tumor growth by H₂ releasing</p> <p>b) Regulated H₂ releasing rate through surface modification</p>	Yangmei Chen, 2015 [8]
Mg@PLGA microspheres/nanospheres	4T1, HeLa, and G422 cell	<p>a) MTT assay: While the cell vitality of the control group with blank PLGA spheres was approximately 100% under laser irradiation, the cell viability of groups containing Mg@PLGA microspheres and nanospheres fell almost linearly with increasing Mg content.</p> <p>b) Fluorescent microscopic images: For <i>in vitro</i> cells, the photothermal property of Mg@PLGA spheres was determined by their absolute Mg concentration rather than their carrier size.</p>	Breast tumor bearing model of nude mice (4T1 cell)	<p>a) The tumor growth curves: Under laser irradiation, the tumor reduction in mice was significant.</p> <p>b) H&E and Masson's trichrome staining: After 16 days of treatments, malignant tissues were ablated by laser irradiation while benign tissues remained unharmed.</p>	PTT effect	Weixiao Zhou, 2020 [35]
MgA: Mg-2Zn-0.3Ca alloy	4T1 cell	<p>a) Dead/Live staining and MTT assay: MgA rods didn't show significant cytotoxicity, while exposed to an AMF, the tumor cells were inhibited growth.</p>	Breast tumor bearing model of nude mice and rabbits (4T1 cell)	<p>a) The tumor growth curves: Tumor tissues of mice in the unimplanted group with and without AMF exposure and mice in the MgA rod-implanted group without AMF exposure showed rapid growth, while tumor tissues of mice in the MgA rod-implanted group with AMF exposure were effectively eliminated.</p> <p>b) H&E staining: Magnetic thermal heating with MgA rods caused severe damage to tumor tissues.</p>	Magnetic hyperthermia effect	Nailing Yang, 2021 [33]

(continued on next page)

Table 4 (continued)

Materials	<i>In vitro</i> studies		<i>In vivo</i> studies		Active ingredients for antitumor effects	Ref.
	Cell type	Results	Animal model (cell type)	Results		
Mg sheets (purity: 99.98 wt%) Mg wires (purity: 99.98 wt%)	HCT116 and HCoEpiC cell	a) CCK-8 assay: Cell mortality was significantly increased with M-H ₂ . b) Flow cytometry: the apoptotic level in the M-H ₂ treatment was much higher than the L-H ₂ . c) mRNA transcriptome analysis: P53 signaling (CDKN1A, SERPINE1, SESN2, FAS, GADD45B and, CCNG2), lysosome signaling (DNASE2, NEU1, LAMP3, and CD68), and apoptosis signaling (TNFRSF10B, IL1A, TNFRSF10C, and FAS). d) Western blot and confocal fluorescence image: The up-regulated P53 activates the mitochondrial apoptosis pathway by H ₂ .	Breast tumor bearing model of nude mice (HCT116 cells)	a) The tumor growth curves: Mg inhibits the tumor growth.	Hydrogen therapy	Rui Zan, 2022 [34]
MgG: decorating platinum on the surface of Mg rods	4T1 cell, CT26 cell, and Rabbit VX ₂ cell	a) Confocal fluorescence image: MgG significantly affect the cellular mitochondrial respiration and cells were damaged after being treated with MgG. b) Flow cytometry: MgG treatment caused significant apoptosis of 4T1 and CT26 cells.	Breast tumor bearing model of nude mice (4T1 cells, Luc-4T1, and CT26 cells)	a) <i>In vivo</i> imaging analysis: MgG inhibit the tumor growth. b) H&E and TUNEL staining: MgG rods induce severe tumor cell apoptosis.	a) H ₂ therapy b) Mg(OH) ₂ residue neutralized the acidic TME.	Nailin Yang, 2022 [85]
MgNF@PEG/PMMVP: pH-sensitive polyethylene glycol-b-(poly(methyl methacrylate)-co-poly(4-vinylpyridine) (PEG-bPMMVP) coated approximately 100 nm of MgNanoFlowers MgNF@PEG/PMMA: pH-insensitive polyethylene glycol-b-(poly(methyl methacrylate) (PEG-b-PMMA) coated MgNanoFlowers	MCF-7 cell, HeLa cell, and MC38 cell	a) CCK-8 assay: The MCF-7 cells showed a notable death in the pH-sensitive MgNF@PEG/PMMVP group. b) Dead/Live staining: The pH-sensitive MgNF@PEG/PMMVP significantly inhibited tumor cell growth. c) Confocal fluorescence image: Severe cell deformation and even rupture were observed in the pH-sensitive MgNF@PEG/PMMVP group, whereas the pH-insensitive MgNF@PEG/PMMA and PBS groups displayed intact cellular morphology.	Breast tumor bearing model of nude mice (MCF-7 cancer cell and MC38 cell)	a) The tumor growth curves: The pH-sensitive MgNF@PEG/PMMVP inhibits the tumor growth. b) Histopathological analyses: In H&E staining, most of the tumor cells from the group treated with pH-sensitive MgNF@PEG/PMMVP died without nuclei or with destroyed cell morphology. In TUNEL staining, a higher level of DNA fragmentation was observed in the pH-sensitive MgNF@PEG/PMMVP group.	H ₂ therapy	Luntao Liu, 2022 [32]

LDH: layered double hydroxide; CCK-8: Cell Counting Kit-8; PTT: photothermal therapy; ROS: Reactive Oxygen Species; TUNEL: TdT-mediated dUTP nick end labeling; AMF: alternating magnetic fields.

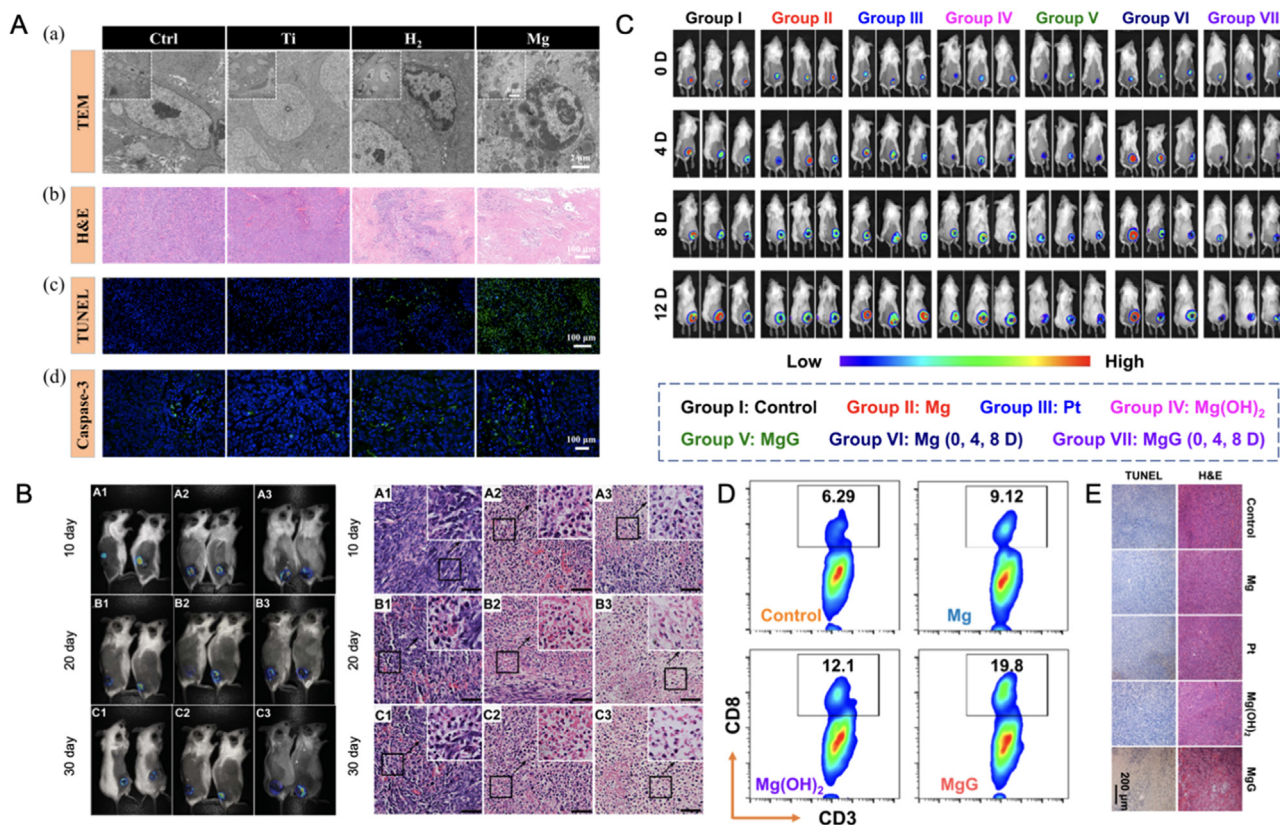


Fig. 5. Representative antitumor effect of Mg alloys for breast cancer: A. (a) TEM photos of the tumor tissues at various scales; (b) H&E images of tumor tissues dissected from each group after different treatments on day 24; (c) Apoptosis was analyzed by TUNEL staining in tumor tissue after 24 days of treatment; (d) Confocal laser scanning microscopy of caspase-3 staining in tumor tissues after different treatments. (Reproduced with permissions from Ref. [34]) B. *In vivo* and H&E images of the tumors in animals at 10, 20, and 30 days post operation. (Control: A1, A2, A3; P-Mg: B1, B2 and B3; AO-HT-Mg: C1, C2 and C3). (Reproduced with permissions from Ref. [8]) C. Bioluminescence images of mice bearing subcutaneous 4T1 tumors expressing firefly luciferase (Luc-4T1) to display the therapeutic efficacy of mice after various treatments. D. The flow cytometric analysis results of CD8 + T cells (CD3 + CD8 +) within the tumors after different treatments. E. Microscopy images of H&E and TUNEL stained tumor slices collected from mice post different treatment groups. (C, D, and E reproduced with permissions from Ref. [85]) (P-Mg: Pure Mg metal; AO-HT-Mg: P-Mg coated with MgO; MgG: Mg-based galvanic cell).

in vivo experimental results of Mg alloys for other tumor types. Table 5 summarizes the specific *in vivo* and *in vitro* experimental results, and related active ingredients of the reported Mg alloys.

Zan et al. [38] invented Mg staples for wound closure after the surgical resection of colorectal tumors to inhibit tumor cells. *In vivo*, the intestinal wounds of rabbits with Mg staples healed gradually with no adverse effects, such as leakage or inflammation; simultaneously, the colorectal tumor cells were inhibited because of the increased concentration of Mg ions and released hydrogen. Peng et al. [40] reported a Mg biliary stent that enables both bile drainage and the treatment of gallbladder cancer. Both the abovementioned Mg biliary stent and staples are degraded directly in the body without removing them at a secondary surgery, which reduces the patient's pain and is expected to be an ideal material for biodegradable implants. Wang et al. [87] combined Mg with gallium-indium alloy which produced a new biomedical material that can adapt to any irregular skin surface. Mg-GaIn plays the antitumor effect of Mg and the plasticity characteristics of

liquid metal simultaneously which shows a good application prospect in melanoma.

5. The antitumor mechanism of magnesium alloys

The antitumor effects of Mg alloys are mainly due to their degradation products, including Mg^{2+} , H_2 , OH^- , and $Mg(OH)_2$. These products mainly inhibit tumor progression by regulating the acidic tumor microenvironment, resisting oxidative stress, resolving tumor inflammation, inhibiting tumor cell proliferation, promoting apoptosis, and reducing migration and invasion directly (Fig. 7). The tumor microenvironment tends to be weakly acidic, with high ROS levels and immunosuppression. The degradation of Mg and Mg alloys directly neutralizes acid, increasing the tumor microenvironment pH, thereby inhibiting tumor progression [90]. In response to the high oxidative stress of tumors, H_2 down-regulates the excessive ROS and improves endogenous antioxidant enzyme levels to inhibit tumor development [91]. Regarding the immune suppression of tumors, the degrada-

Table 5

Summary of the *in vitro*, *in vivo* studies and active ingredients of the Mg alloys for anti other types of tumors (except bone and breast) applications.

Material	<i>In vitro</i> studies		<i>In vivo</i> studies		Active ingredients for antitumor effects	Ref.
	Cell type	Results	Animal model (cell type)	Results		
Chit-Mg MPs	Hepa1-6 cell	a) Biocompatibility: No mortality was seen in cells incubated with the particles.	Liver tumor bearing model of nude mice (Hepa1-6 cell)	a) Histological analysis: Tumor tissue was extensively harmed.	PTT effect	Robert. C. Martin, 2016 [41]
EGaIn: gallium-based liquid metal Mg-GaIn group: EGaIn mixed with Mg particles + Laser	C8161 cell: for antitumor effect, HaCaT cell: for cytotoxicity test	a) CCK-8 assay: Mg-GaIn reaction medium showed no significant cytotoxicity to C8161 cell and HaCaT cell. b) Live/Dead staining: Similar results to CCK-8 assay.	Melanoma bearing model of nude mice (C8161 cell)	a) The tumor growth curves: After three times treatments, PTT with either Mg-GaIn + laser or laser alone displayed remarkably higher tumor growth retardation compared to the blank control group, Mg-GaIn group and EGaIn group. b) MR imaging: The tumor shape of Mg-GaIn + laser group and laser group was changed into flat shape at Day 6. The MR image with MgGaIn + laser treatment at Day 13 detected no tumor at tumor site while tumor still existed in the laser group. c) H&E staining: Less tumor cell was observed in MgGaIn + laser group.	PTT effect	Xuelin Wang, 2018 [87]
Mg-2.0%Ag (2 wt% Ag) Mg-4.0%Ag (4 wt% Ag) ECAP: Equal-channel angular pressing IS: initial state	K562 cell	a) Lactate dehydrogenase (LDH) level test: The LDH activity in the wells with samples of the alloys in the initial state was higher than in the wells containing samples of the ECAP-processed alloys. Samples of the alloy with a higher content of silver induced a greater LDH release in the culture medium. b) Cell viability assay: The samples of the alloys in the initial state inhibited the viability of tumor cells more efficiently than ECAP-processed ones. Samples containing 4% Ag were found to be more toxic to tumor cells. c) Tumor cells apoptosis test: Compared to ECAP group, the concentration of Annexin V (+) cells and Caspase 3/7 (+) cells were higher in initial state group. Samples containing 4% Ag were more active than those with the corresponding processing history but a lower concentration of silver. d) Oxidative stress assess: Compared to ECAP group, the NO and ROS level were higher in initial state group.	–	–	a) The accelerated destruction of cell membranes leading to an increased release of LDH. b) Initiation of oxidative stress initiation. c) Led the cell apoptosis.	Yuri Estrin, 2019 [88]

Table 5 (continued)

Material	<i>In vitro</i> studies		<i>In vivo</i> studies		Active ingredients for antitumor effects	Ref.
	Cell type	Results	Animal model (cell type)	Results		
Mg–Zn–Y–Nd	Eca109 cell, L929 cell, Het-1A cell, macrophages	a) AO/EB staining images: Mg–Zn–Y–Nd significantly inhibited tumor cells.	–	–	Strong inhibition of esophageal cancer related pathological cells.	Shuo Wang, 2020 [16]
Mg wires Mg sheets	SKOV3 cell	<p>a) Live/Dead staining: The number of dead cells increased as the concentration of Mg²⁺ exceeds 20 mM and when pH value increased.</p> <p>b) CCK-8 assay: The tumor cells proliferated more slowly as the concentration of Mg²⁺ and the pH value increased.</p> <p>c) Apoptosis Analysis: When the concentration of Mg²⁺ in the medium reached 30 mM, the apoptotic rate of SKOV 3 cells on the 3rd day was 2.3 times higher than that of the control group (0 Mg²⁺). The percentage of apoptotic cells was also raised with the pH value of culture medium, up to 34.6% in the culture medium with a pH value of 8.3.</p> <p>d) Cell Cycle Analysis: While the variation in the pH value (from 7.4 to 8.3) or exposure to H₂ (80 μ L/h) do not affect the cell cycle of SKOV3 cells, the addition of excessive Mg²⁺ could increase G0/G1 phase cells.</p>	Ovarian cancer bearing model of nude mice (SKOV3/Luc cell)	<p>a) The tumor growth curves: The Mg wire-pierced mice group showed a significantly suppressed tumor growth with better bodyweight maintaining compared to the Ti-implanted and the implant-free control groups.</p> <p>b) <i>In Vivo</i> Imaging Analysis: A significant decrease was detected in the tumor volume of Mg-treated mice compared to Ti-treated mice and a control group on the 25th day after Mg implantation.</p> <p>c) Histology Examination: H&E staining showed more shrinkage of tumor cells and absence of cell nuclei was observed in the Mg-implanted mice group. Compared to the other treatment groups, the amount of TUNEL-positive cells was significantly increased in the Mg group.</p>	<p>a) The quenching of free radicals induced by H₂ in tumor cells.</p> <p>b) Excessive Mg²⁺ (>10 mM) could inhibit the proliferation of tumor cells by arresting the cell cycles in the G0/G1 phase.</p>	Shuang Qiao, 2020 [36]

(continued on next page)

Table 5 (continued)

Material	<i>In vitro</i> studies		<i>In vivo</i> studies		Active ingredients for antitumor effects	Ref.
	Cell type	Results	Animal model (cell type)	Results		
WE43: Mg–3.56%Y–2.20%Nd–0.47%Zr ECAP: equal channel angular pressing	LNCaP cell, MDA-MB231 cell	<p>a) MTT assay: In the ECAP-processed state, WE43 exhibited a more pronounced cytotoxic activity than in the homogenized state.</p> <p>b) Apoptosis Analysis: Contacting with the alloy caused the induction of apoptosis of both tumor cell lines. The effect of WE43 was more pronounced for the ECAP-processed samples.</p> <p>c) Oxidative stress assess: The amount of oxygen radicals expressing the concentration of ROS (+) cells decreased.</p> <p>d) Bcl-2(+) tumor cells concentration test: A significant decrease was seen in the concentration of Bcl-2 (+) cells during the incubation of LNCaP tumor cells with the samples of both states of the alloy—by 9–14% compared with the control (cells cultured without WE43 alloy).</p>	–	–	<p>a) A relatively fast degradation of the material would enhance the release of RE elements, thus supporting the antitumor activity.</p> <p>b) The biodegradation-induced rise of the pH level of the culture medium and caused the osmotic shock of tumor cells.</p> <p>c) The greater antitumor activity of ECAP-processed WE43 might be associated with the grain refinement this process produces, while also causing precipitation of the RE-enriched phase Mg₄₁Nd₅.</p> <p>d) The induction of apoptosis.</p>	Natalia Anisimova, 2020 [37]
Mg-6% Ag Mg-10%Gd	PC-3 cell	<p>a) Lactate dehydrogenase (LDH) level test: The anti-tumor cell activity of the alloy specimens in the ECAP-processed state was more pronounced than in the homogenized one. Mg-10%Gd in both states produced a greater effect than Mg-6%Ag.</p> <p>b) Ki67(+) cells assay: The number of Ki-67(+) cells decreased by 97% and 87% for Mg-10%Gd and Mg-6%Ag, respectively.</p>	Melanoma bearing model of C57BL/6 mice (B16 murine melanoma cells)	<p>a) CT examination: The destruction in the tumor node was as large as some 40% of its volume with implanted Mg-10%Gd ECAP pins, significantly larger than the other groups.</p> <p>b) The tumor growth curves: The decrement of the volume of the tumor tissue associated with the anti-tumor effect of the alloys considered was 30%, 22%, and 8% for Mg-10%Gd ECAP, Mg-6%Ag ECAP, and Mg-10%Gd homogenization, respectively.</p> <p>c) Ki-67(+) cells test: The largest drop in the number of Ki-67(+) cells was observed in tumors in mice with implanted pins made from ECAP-processed Mg alloys.</p>	The synergistic effect of severe effects and the influence of the eluted gadolinium ions on the tumor cells.	Natalia Anisimova, 2021 [86]

Table 5 (continued)

Material	<i>In vitro</i> studies		<i>In vivo</i> studies		Active ingredients for antitumor effects	Ref.
	Cell type	Results	Animal model (cell type)	Results		
As-cast Mg	RBE cell	<p>a) CCK-8 assay: The proliferation of RBE cells was significantly inhibited in the Mg group compared with the Ti group.</p> <p>b) Apoptosis analysis: The Mg extract accelerated apoptosis of RBE cells.</p> <p>c) Cell adhesion test: A dramatically greater number of adherent cells on the Ti plates than on the Mg plates at each time point.</p> <p>d) Immunofluorescence (IF) of cytoskeletal actin: Either 4 or 24 h after incubation, there were no intact dyed tumor cells on the Mg plates while tumor cells grew vigorously on the surfaces of Ti plates.</p>	H22 tumor bearing model of nude mice (Hepatoma-22 cell)	<p>a) The tumor growth curves: The tumor volume was significantly greater in the Ti than in the Mg group.</p> <p>b) Histopathological analyses: On H&E-stained images, tumor cells shrank, and their nuclei disappeared around the implanted Mg wire, indicating cytotoxicity of Mg to tumor cells. TUNEL staining showed significantly more apoptotic cells, which were stained brown, in the Mg group than in the Ti and control groups. IHC staining results showed that the expression of HIF-1α was slightly inhibited in the Mg group compared with the Ti group; its downstream protein CAIX had significantly lower expression in the Mg group than in the Ti and control groups.</p>	<p>a) The Mg extract inhibited proliferation and induced apoptosis of RBE cells.</p> <p>b) A Mg plate inhibited cell adhesion and destroyed the cytoskeleton in the process of biodegradation.</p> <p>c) Mg wires promoted tumor apoptosis and inhibited the expressions of HIF-1α and CAIX.</p>	Tian Li, 2021 [89]
Mg wires	SGC-996 cell, GBCSD cell	<p>a) CCK-8 assay: The magnesium wire coculture group had an inhibitory effect on gallbladder cancer cells, and as the number of magnesium wires increases, the inhibitory effect on gallbladder cancer cells was enhanced.</p> <p>b) Apoptosis analysis: When the Mg²⁺ concentration of the culture medium was 10 and 20 mmol/L, the apoptosis rate of gallbladder cancer cells was not significantly different from that of the control group, but when the Mg²⁺ concentration was 30 mmol/L, the apoptosis rate was significantly different from that of the control group (0 Mg²⁺). With the increase of pH value (pH \geq 7.8), the apoptosis rate of gallbladder cancer cells began to rise.</p> <p>c) Cell cycle analysis: When gallbladder cancer cells were cultured in a medium containing Mg²⁺ for 48 h, the proportion of cells in the G0/G1 phase was significantly lower than that of the control group (0 Mg²⁺). With the increase of the pH value of the medium, the proportion of cells in the G0/G1 phase increased.</p>	Gallbladder tumor bearing model of nude mice (SGC-996 cell)	<p>a) The tumor growth curves: At 24 days of implantation, the volume and weight of xenograft tumors of the Ti wire group showed no significant difference with the control group. However, at 24 days of implantation, the tumor weights of the 1 Mg wire group and the 3 Mg wire group were significantly lower than those of the control group (without implantation).</p> <p>b) Histopathological analyses: Compared with the control group and the Ti wire implantation group, the histology of the main organs after the Mg wire implantation was not abnormal.</p>	The degradation products of Mg could significantly inhibit the growth of gallbladder cancer cells and promote their apoptosis.	Hongzhou Peng, 2021 [40]

(continued on next page)

Table 5 (continued)

Material	<i>In vitro</i> studies		<i>In vivo</i> studies		Active ingredients for antitumor effects	Ref.
	Cell type	Results	Animal model (cell type)	Results		
Mg staples Mg wires	LS174T cell	a) CCK-8 assay: Mg inhibited the tumor cell growth with the Mg content increasing. b) Live/Dead staining: Mg inhibited the tumor cell growth with the Mg content increasing. c) Apoptosis analysis: The apoptotic rate of LS174T cells dramatically elevated as the number of Mg staples increases. d) Cell cycle analysis.: The percentage of the distribution in the G0/G1 phase increased as the number of Mg staples increases. e) Cell migration analysis: The Mg group effectively inhibited the cell migration compared to the control group.	Colorectal cancer bearing model of nude mice (LS174T cell)	a) The tumor growth curves: Mg staples inhibited the tumor growth. b) Histopathological analyses: The number of tumor cells colored in purple was more than that in the Mg staple group.	Mg staples inhibit growth and migration and induce apoptosis of colorectal tumor cells.	Rui Zan, 2021 [38]
LMM@BSA: Mg-Mn-Al alloy-MOS ₂ -bovine serum albumin LMM@BSA/Ce6: Mg-Mn-Al alloy-MOS ₂ -bovine serum albumin-chlorin e6	L929 cell: for biocompatibility, HT29 cell: for antitumor effect	a) CCK-8 assay: L929 cells grown with LMM@BSA clay nanosheets for 24 h maintained greater than 90% viability; With the LMM@BSA fixed at 500 g/ mL, the HT29 cells' viability rapidly decreased as power density increased, reaching a low viability of $14.6 \pm 0.1\%$. b) Live/Dead staining: Cellular vitality of HT29 cells treated with LMM@BSA and LMM@BSA/Ce6 nanosheets dropped after laser exposure to $86.6 \pm 1.7\%$ and $41.7 \pm 3.3\%$, respectively. c) Hemolytic percentage (HP) test: Under nanosheet concentrations of 0–500 g/mL, the HPs of experimental samples were found to be lower than 2%. d) Ce6 upload test: When Ce6 (PTA) and LMM@BSA were combined, the production of ROS was enhanced.	Colorectal tumor bearing model of nude mice (HT29 cell)	The tumor growth curves: Following the combined PDT and PTT, the tumor volume of the LMM@BSA/Ce6 group decreased to roughly 40% of the original (injected with 20 μ L), and they were eliminated (injected with 200 μ L)	a) PTT effect b) PDT effect	Jiayan Zhao, 2021 [39]
Mg (pure: 99.95 wt%) Mg–6Ag (Mg with 6 wt% Ag)	RF Fibroblasts: for cytotoxicity effect Saos-eGFP cell: for antitumor effect	a) Immunofluorescence: The number of cancer cells on Mg and Mg–6Ag was significantly lower. b) Ki-67 and p38 immunostaining: Mg-based materials inhibit Saos-eGFP cell proliferation. c) ELISA: elevated IL-8 secretion from the coculture on Mg-based materials.	–	–	The Mg degradation dependent pH increased.	Philipp Globig, 2022 [24]

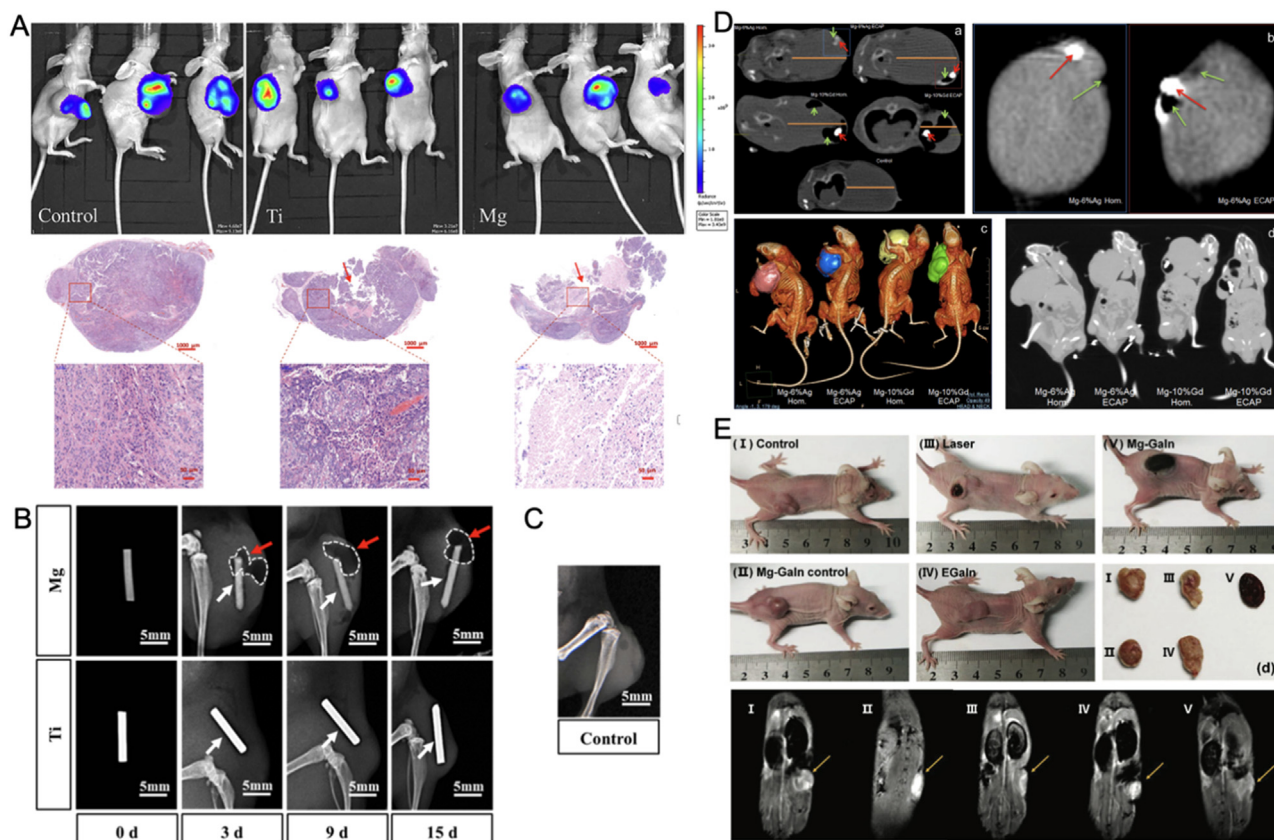


Fig. 6. Representative other types of tumors: A. Bioluminescence and H&E stained images of ovarian tumor-bearing mice implanted with and without metallic wires on the 25th day. Red arrow indicated the position of Mg or Ti implantation. (Reproduced with permissions from Ref. [36]) B. Soft X-ray photography of Hepatoma tumor-bearing mice with Mg and Ti wires on the 3rd, 9th, and 15th days. The white arrows show Mg and Ti wires, and the red arrows show the gas (white-dashed) around Mg wires. C. Soft X-ray photography of the blank control group on the 15th day. (B and C reproduced with permissions from Ref. [89]) D. Longitudinal and transversal CT scans of tumoral nodes in melanoma tumor-bearing mice with inoculated melanoma after 10 days of intratumorally implantation of alloy pins. An orange line marks the diameter of a tumoral node, green arrows indicate gas bubbles, and a red arrow points to the alloy pin. (a) A transversal section of the body of a mouse with an inoculated tumor; (b) a longitudinal section of the tumor for Mg-6%Ag Hom. and Mg-6%Ag ECAP; (c) CT images of tumoral nodes containing gas accumulated in cavities in mice with implanted Mg-6%Ag and Mg-10%Gd alloy pins. The images represent 3D rendering of the reconstructed tumoral nodes of the groups of mice; (d) longitudinal section of tumor-bearing mice with different alloy implants. (Reproduced with permissions from Ref. [86]) E. The 6th day photographs of melanoma tumor-bearing mice after three times treatments. d) The resected tumor tissues from tumor-bearing mice after three times treatments. e) The 6th day MR images. (Reproduced with permissions from Ref. [87]) (HOM.: homogenized; ECAP: Equal-channel angular pressing).

tion products Mg^{2+} and H_2 reduce inflammation, although the specific mechanism needs to be explored [92,93]. Mg^{2+} and H_2 also directly inhibit tumor cell proliferation and promote apoptosis [94,95]. Therefore, Mg alloys may be potential biomaterials for antitumor treatment. Here, we summarize the antitumor mechanisms of the active components of Mg, including Mg^{2+} , H_2 , OH^- , and $Mg(OH)_2$.

5.1. Mechanism of Mg^{2+} on tumor inhibition

The corrosion product Mg^{2+} inhibits tumor progression mainly by inhibiting tumor cell proliferation, promoting apoptosis, suppressing migration and invasion, and improving tumor inflammation. Specifically, Mg^{2+} inhibits tumor proliferation through transient receptor potential melastatin7 (TRPM7) related signaling pathway and protein phosphatase 1D (PPM1D) [18,96,97], and promotes tumor apoptosis through AKT/mTOR and Bax signaling pathways [98].

Mg^{2+} may against tumor invasion and metastasis by inhibiting the tumor necrosis factor- α (TNF- α)/interleukin-1 (IL-1)/NF- κ B signaling pathway [60,99]. Moreover, Mg^{2+} improves tumor inflammation by reducing the release of inflammatory factors such as IL-1 α , IL-6, NO, and vascular cell adhesion molecule (VCAM) [100] (Fig. 8). Additionally, Mg^{2+} also regulates protein endocytosis and channel proteins to inhibit tumor angiogenesis and multi-drug resistance [18].

5.2. Mechanism of H_2 on tumor inhibition

H_2 has a surprising ability to inhibit tumor progression by inhibiting tumor proliferation, promoting apoptosis, improving inflammation, and regulating oxidative stress (Fig. 9). Specifically, H_2 inhibits tumor cell proliferation via the PI3K/AKT signaling pathway [101] and promotes tumor cell apoptosis via NF- κ B-related signaling pathway [95]. de-

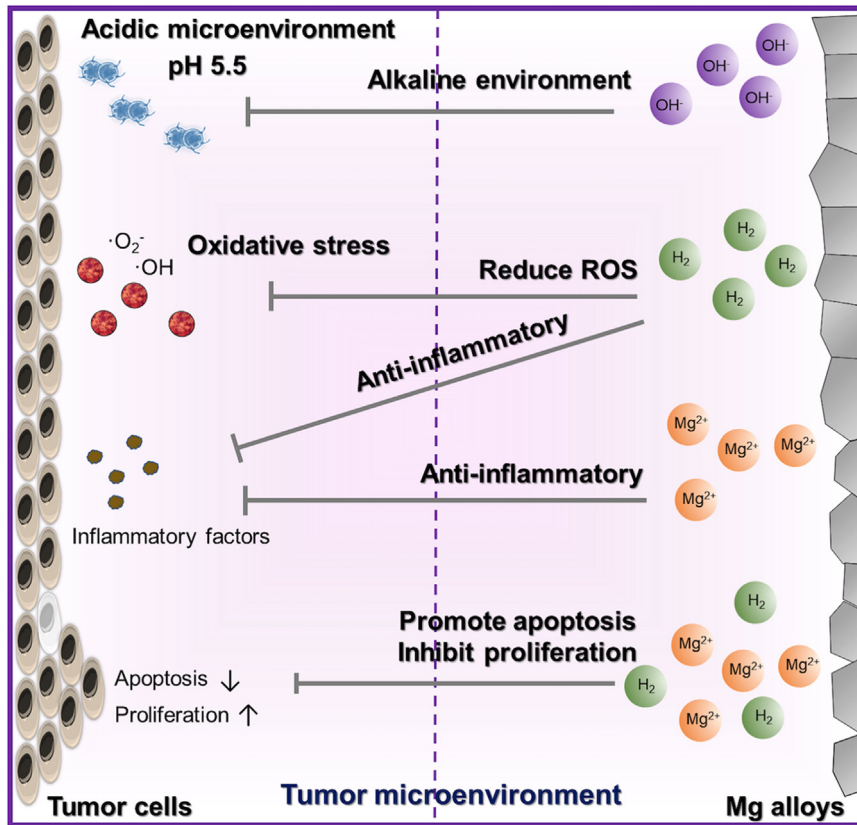


Fig. 7. Tumors biological characteristics and Mg alloys material properties.

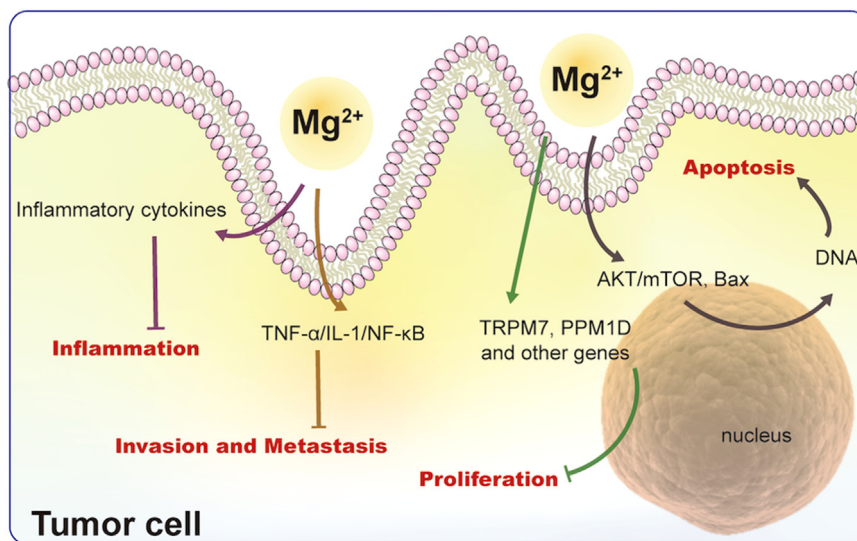
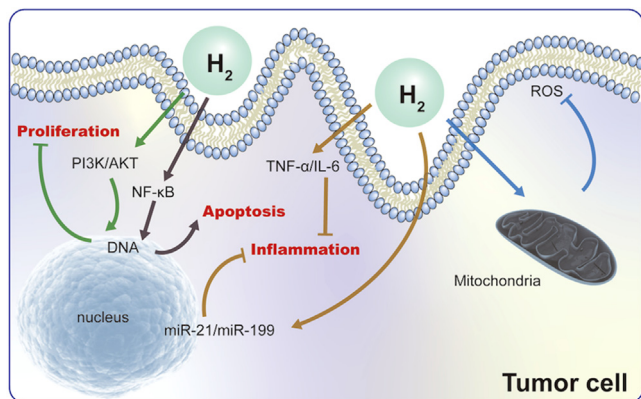
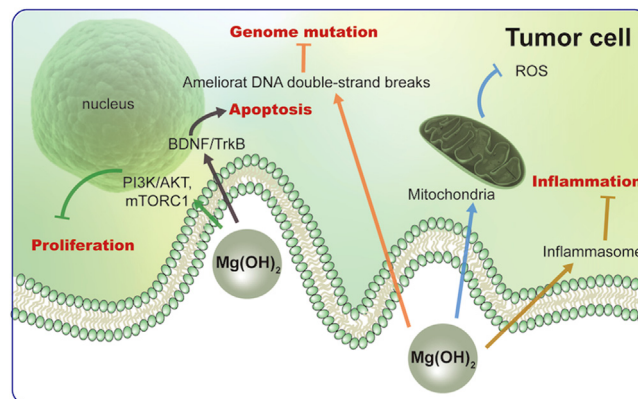
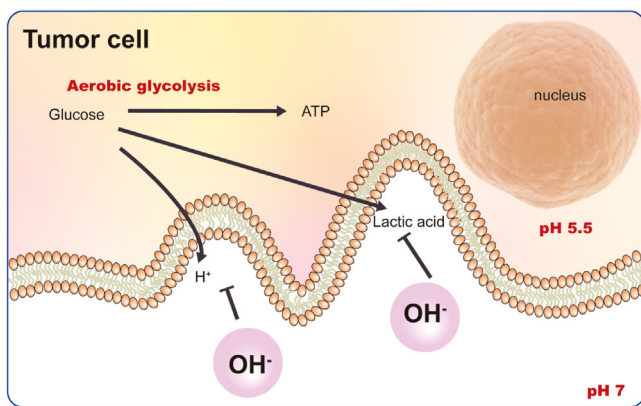


Fig. 8. Antitumor mechanisms of Mg²⁺.

creasing the number of tumor cells sharply. H₂ also downregulates proinflammatory cytokines (e.g., TNF-α and IL-6) to alleviate tumor inflammation [102] and also regulates microRNA (e.g., miR-21 and miR-199) to control tumor inflammation [103]. In terms of oxidative stress, H₂ inhibits vascular endothelial growth factor (VEGF) and ERK signaling downregulation by reducing excessive ROS [104] and activates the

body's own antioxidant system through the production of endogenous antioxidants, such as catalase (CAT) and superoxide dismutase (SOD) [105]. H₂ also regulates oxidative stress and the Nrf2 signaling pathway to ameliorate genomic instability and mutation in tumor cells [106]. Therefore, H₂, the degradation product of Mg and Mg alloys, has a potential role in tumor treatment.

Fig. 9. Antitumor mechanisms of H₂.Fig. 11. Antitumor mechanisms of Mg(OH)₂.Fig. 10. Antitumor mechanisms of OH⁻.

5.3. Mechanism of OH⁻ on tumor inhibition

Aerobic glycolysis is the main method of energy production in tumor cells. One molecule of glucose is converted to two molecules of lactic acid, two molecules of H⁺ and two molecules of ATP. The accumulated lactic acid and excess H⁺ diffuse into the extracellular matrix forming an acidic microenvironment that promotes cell proliferation and invasion [107]. Therefore, alkalinizing the tumor microenvironment is an effective antitumor strategy. Notably, during the degradation process of Mg, the OH⁻ generated by cathodic reactions and the decomposition of Mg(OH)₂ neutralizes acidic substances, increasing the pH value, and thereby inhibiting tumor progression (Fig. 10).

5.4. Mechanism of Mg(OH)₂ on tumor inhibition

The corrosion product Mg(OH)₂ also achieves tumor-suppressive effects through various pathways, which include inhibiting tumor cell proliferation, promoting tumor cell apoptosis, and regulating tumor-related inflammation (Fig. 11). Mg(OH)₂ may inhibit the replicative immortality of tumor cells by inhibiting the PI3K/AKT signaling pathway [18,108] and activate mTORC1 to inhibit tumor cell proliferation [18,109]. In terms of regulating tumor cell death, Mg(OH)₂ may also promote tumor cell apoptosis by reg-

ulating the BDNF/TrkB signaling pathway [18,110]. Moreover, Mg(OH)₂ may inhibit ROS production [18] and suppress tumor-associated inflammation by inhibiting the inflammasome [18,111]. Finally, in terms of genomic instability and mutation, Mg(OH)₂ may ameliorate DNA double-strand breaks to inhibit tumor progression [18,112]. Therefore, Mg has excellent application prospects in inhibiting tumors and improving the tumor microenvironment.

6. Challenges and perspectives

In clinical practice, malignant tumors are traditionally treated via surgical resection followed by chemotherapy/radiation to kill the remaining tumor cells. Moreover, the tissue defects caused by resection of the primary focus, substantially decrease survival rates and have a devastating impact on patients' lives. Therefore, there is an urgent need for highly selective, non-invasive treatments and advanced biomaterials that can simultaneously fight tumors and promote osteogenesis.

Studies confirm the positive contribution of appropriate external stimulation to tumor treatment, including thermal stimulation [7], electrical stimulation [113], magnetic stimulation [114], and light stimulation [69], and the pH response [115]. The use of Mg alloys combined with near infrared light, pH modulation, and other external stimulation has achieved good efficacy for tumor treatment. However, because the external stimulation conditions are strictly limited, unreasonable use may produce irreversible damage to the surrounding healthy tissues. Therefore, the precise control of Mg alloys and stimulation is needed. When Mg alloys are combined with PTT, normal tissue can tolerate short periods of irradiation. If the duration and power of the irradiation are not controlled, the deep tissue cannot be heated with pinpoint precision, such that the heat may have harmful effects on normal cells and normal tissue surrounding the tumor [77,116]. The irradiation power and duration should be adjusted carefully to achieve a suitable target temperature. As reported, the temperature of local thermotherapy needs to exceed 50 °C to achieve an antitumor effect, but hyperthermia exceeding 50 °C can cause irreversible DNA and protein denaturation in cancerous lo-

cations. While the temperature range suitable for osteogenic differentiation is 40–42 °C. Thus, precise temperature control is necessary during PTT in conjunction with Mg alloys. A temperature-sensitive Mg alloy with a large temperature conversion range combined with a gradient-controlled heating process will likely achieve the goals of two-stage antitumor treatment.

The biosafety of an implanted material is an important consideration. On the one hand, attention should be paid to regulate the release of degradation products to achieve better antitumor effects. On the other hand, Hepatic and renal clearance, the clearance cycle and complete degradation time, and the acute and chronic toxicity of degradation products of Mg alloys should be evaluated to ensure their biosafety before clinical application and further clinical translation. It is also necessary to consider how to modify the size, surface morphology, internal structure, and surface charge of Mg alloys to minimize nonspecific damage to normal cells.

Declaration of competing interest

The authors declare that they have no known competing financial interests or personal relationships that could have appeared to influence this paper.

Acknowledgement

This study was supported by the National Key R&D Program of China [grant number 2021YFC2400700], the National Natural Science Foundation of China [grant numbers 82170929, 81970908] and the Beijing Natural Science Foundation [L222090, L222030].

References

- [1] P.E. Clark, F.M. Torti, *Clin. Orthop. Relat. Res.* (415 Suppl) (2003) S148–S157.
- [2] Y. Jj, P. Cb, K K, *Cell Res.* 15 (1) (2005) 57–62 (-1001-0602(Print)):Tppublish, doi:10.1038/sj.cr.7290266.
- [3] J. Shen, W. Zhang, R. Qi, et al., *Chem. Soc. Rev.* 47 (6) (2018) 1969–1995.
- [4] P.Y. Teo, W. Cheng, J.L. Hedrick, et al., *Adv. Drug. Deliv. Rev.* 98 (2016) 41–63.
- [5] C.H. June, R.S. O'connor, O.U. Kawalekar, et al., *Science* 359 (6382) (2018) 1361–1365.
- [6] A. Ribas, J.D. Wolchok, *Science* 359 (6382) (2018) 1350–1355.
- [7] M. Chang, Z. Hou, M. Wang, et al., *Adv. Mater.* 33 (4) (2021) e2004788.
- [8] Y. Chen, M. Xiao, H. Zhao, et al., *J Mater Chem B* 3 (5) (2015) 849–858.
- [9] I. Obiorah, V.C. Jordan, *Maturitas* 70 (4) (2011) 315–321.
- [10] Y.F. Zheng, X.N. Gu, F. Witte, *Mater. Sci. Eng. R. Rep.* 77 (2014) 1–34.
- [11] Y. Huang, F. Jin, Y. Funato, et al., *Sci. Adv.* 7 (7) (2021).
- [12] H. Lin, S. Shi, X. Lan, et al., *Small Methods* 5 (9) (2021) e2100536.
- [13] R. Waksman, R. Pakala, P.K. Kuchulakanti, et al., *Catheter. Cardiovasc. Interv.* 68 (4) (2006) 607–617 discussion 618–9.
- [14] Y. Liu, Y. Zheng, X.H. Chen, et al., *Adv. Funct. Mater.* 29 (18) (2019) 1805402.
- [15] P. Ding, Y. Liu, X. He, et al., *Bioact. Mater.* 4 (2019) 236–244.
- [16] S. Wang, X. Zhang, J. Li, et al., *Bioact. Mater.* 5 (1) (2020) 1–8.
- [17] D. Zhao, F. Witte, F. Lu, et al., *Biomaterials* 112 (2017) 287–302.
- [18] B. Xu, Y. Song, K. Yang, et al., *J. Magnes. Alloys* 11 (3) (2023) 763–775.
- [19] Y. Dai, Y. Tang, X. Xu, et al., *J. Biomed. Mater. Res. B Appl. Biomater.* 107 (8) (2019) 2537–2548.
- [20] S. Kannan, R. Nallaiyan, *ACS Appl. Bio Mater.* 3 (7) (2020) 4408–4416.
- [21] C. Shuai, L. Liu, Y. Yang, et al., *Appl. Sci.* 8 (11) (2018) 2109.
- [22] Y. Wu, G. He, Y. Zhang, et al., *Sci. Rep.* 6 (2016) 21736.
- [23] P. Globig, R. Madurawala, R. Willumeit-Romer, et al., *Bioact. Mater.* 19 (2023) 594–610.
- [24] P. Globig, R. Willumeit-Romer, F. Martini, et al., *Bioact Mater* 16 (2022) 320–333.
- [25] J. Li, P. Zhou, L. Wang, et al., *J. Mater. Sci. Mater. Med.* 32 (4) (2021) 43.
- [26] M. Li, M. Yao, W. Wang, et al., *Acta Biomater.* 121 (2021) 682–694.
- [27] L. Liu, F. Peng, D. Zhang, et al., *J. Magnes. Alloys* 10 (11) (2022) 3031–3040.
- [28] J. Long, W. Zhang, Y. Chen, et al., *Biomaterials* 275 (2021) 120950.
- [29] A. Milenin, M. Wrobel, P. Kustra, et al., *Materials* 14 (21) (2021).
- [30] D. Zhang, S. Cheng, J. Tan, et al., *Bioact. Mater.* 17 (2022) 394–405.
- [31] R. Zan, W. Ji, S. Qiao, et al., *Sci. China Mater.* 64 (4) (2021) 1007–1020.
- [32] L. Liu, Y. Wu, J. Ye, et al., *Chem.* 8 (11) (2022) 2990–3007.
- [33] N. Yang, F. Gong, L. Cheng, et al., *Natl. Sci. Rev.* 8 (1) (2021) nwaal22.
- [34] R. Zan, H. Wang, W. Cai, et al., *Bioact. Mater.* 9 (2022) 385–396.
- [35] W. Zhou, Y. Zhang, S. Meng, et al., *Small Methods* 5 (2) (2021) e2000920.
- [36] S. Qiao, Y. Wang, R. Zan, et al., *ACS Biomater. Sci. Eng.* 6 (3) (2020) 1755–1763.
- [37] N. Anisimova, M. Kiselevskiy, N. Martynenko, et al., *J. Biomed. Mater. Res. B Appl. Biomater.* 108 (1) (2020) 167–173.
- [38] R. Zan, H. Wang, J. Ni, et al., *ACS Biomater. Sci. Eng.* 7 (11) (2021) 5269–5278.
- [39] J. Zhao, H. Wu, J. Zhao, et al., *J. Nanobiotechnol.* 19 (1) (2021) 36.
- [40] H. Peng, K. Fan, R. Zan, et al., *Acta Biomater.* 128 (2021) 514–522.
- [41] R.C. Martin, E. Locatelli, Y. Li, et al., *J. Mater. Chem. B* 4 (2) (2016) 207–211.
- [42] O. Warburg, *Science* 123 (3191) (1956) 309–314.
- [43] C. Chen, L. Bai, F. Cao, et al., *Oncogene* 38 (23) (2019) 4527–4539.
- [44] K. Fischer, P. Hoffmann, S. Voelkl, et al., *Blood* 109 (9) (2007) 3812–3819.
- [45] J.P. Schöning, M. Monteiro, W. Gu, *Clin. Exp. Pharmacol. Physiol.* 44 (2) (2017) 153–161.
- [46] K. Graham, E. Unger, *Int J Nanomedicine* 13 (2018) 6049–6058.
- [47] W. Liu, B. Wang, M. Zhou, et al., *Antioxid. Redox Signal.* (2023) ja.
- [48] A.J. Boutilier, E. Sawa, S.F. Macrophage, *Int. J. Mol. Sci.* 22 (13) (2021).
- [49] T.L. Whiteside, *Immunotargets Ther.* 4 (2015) 159–171.
- [50] S. Yin, W. Duan, W. Liu, et al., *Corros. Sci.* 166 (2019) 108419.
- [51] R.C. Zeng, J. Zhang, W.J. Huang, et al., *Trans. Nonferrous Metals Soc. China* 16 (B02) (2006) s763–s771.
- [52] R. Ambat, N.N. Aung, W. Zhou, *Corros. Sci.* 42 (8) (2000) 1433–1455.
- [53] Y. Song, D. Shan, R. Chen, et al., *Corros. Sci.* 52 (5) (2010) 1830–1837.
- [54] X. Liu, D. Shan, Y. Song, et al., *Electrochim. Acta* 56 (5) (2011) 2582–2590.
- [55] R. Tunold, H. Holtan, M.B.H. Berge, et al., *Corros. Sci.* 17 (4) (1977) 353–365.
- [56] B P M A, A B H, B D E, et al., *J. Alloys Compd.* 777 (2019) 835–849.
- [57] A. Atrens, N. Winzer, W. Dietzel, *Adv. Eng. Mater.* 13 (1–2) (2011).
- [58] A. Atrens, *Stress Corros. Cracking* (2011) 341–380.
- [59] T.M. Yue, H.U. Ha, N.J. Musson, *J. Mater. Sci.* 30 (9) (1995) 2277–2283.
- [60] *Int. J. Fatigue*, 1997, 19 (5):438.
- [61] H.E. Friedrich, B.L. Mordike, *Magnesium Technology*, 212, Springer, 2006.

- [62] Y. Wan, G. Xiong, H. Luo, et al., *Mater. Des.* 29 (10) (2008) 2034–2037.
- [63] I.S. Berglund, H.S. Brar, N. Dolgova, et al., *J. Biomed. Mater. Res. B Appl. Biomater.* 100 (6) (2012) 1524–1534.
- [64] G. He, Y. Wu, Y. Zhang, et al., *J. Mater. Chem. B* 3 (32) (2015) 6676–6689.
- [65] N. Birbilis, M.A. Easton, A.D. Sudholz, et al., *Corros. Sci.* 51 (3) (2009) 683–689.
- [66] J. Ritter, S.S. Bielack, *Ann. Oncol.* 21 (Suppl 7) (2010) vii320–5.
- [67] M. Kansara, M.W. Teng, M.J. Smyth, et al., *Nat. Rev. Cancer* 14 (11) (2014) 722–735.
- [68] H. Shao, S. Cheng, M. Yao, et al., *Regen. Biomater.* 8 (6) (2021) rbab053.
- [69] Y. Liu, P. Bhattarai, Z. Dai, et al., *Chem. Soc. Rev.* 48 (7) (2019) 2053–2108.
- [70] L. Zou, H. Wang, B. He, et al., *Theranostics* 6 (6) (2016) 762–772.
- [71] A.M. Alkilany, L.B. Thompson, S.P. Boulous, et al., *Adv. Drug. Deliv. Rev.* 64 (2) (2012) 190–199.
- [72] S.H. Hu, R.H. Fang, Y.W. Chen, et al., *Adv. Funct. Mater.* 24 (26) (2014) 4144–4155.
- [73] Y. Ma, X. Liang, S. Tong, et al., *Adv. Funct. Mater.* 23 (7) (2013) 815–822.
- [74] V. Shanmugam, S. Selvakumar, C.S. Yeh, *Chem. Soc. Rev.* 43 (17) (2014) 6254–6287.
- [75] V.P. Sankara Narayanan, S.G. Kathirason, P. Elango, et al., *RSC Adv.* 13 (24) (2023) 16724–16740.
- [76] H. Ma, C. Jiang, D. Zhai, et al., *Adv. Funct. Mater.* 26 (8) (2016) 1197–1208.
- [77] Z. Wan, P. Zhang, L. Lv, et al., *Theranostics* 10 (25) (2020) 11837–11861.
- [78] X. Wang, Y. Liu, M. Zhang, et al., *Adv. Healthc. Mater.* 10 (21) (2021) e2101181.
- [79] X. Wang, J. Xue, B. Ma, et al., *Adv. Mater.* 32 (48) (2020) e2005140.
- [80] D. Zhang, J. Tan, R. Xu, et al., *Small* 19 (5) (2023) e2204852.
- [81] S. Ramazi, M. Salimian, A. Allahverdi, et al., *Sci. Rep.* 13 (1) (2023) 8844.
- [82] P. Kumar, B. Mangla, S. Javed, et al., *Front. Pharmacol.* 14 (2023) 1149554.
- [83] C. Pu, Y. Liu, R. Deng, et al., *Bioorg. Chem.* 138 (2023) 106637.
- [84] Z. Guo, W. Xie, J. Lu, et al., *Biomater. Sci.* 9 (17) (2021) 5928–5938.
- [85] N. Yang, F. Gong, B. Liu, et al., *Nat. Commun.* 13 (1) (2022) 2336.
- [86] N. Anisimova, M. Kiselevskiy, N. Martynenko, et al., *Mater. Sci. Eng. C Mater. Biol. Appl.* 130 (2021) 112464.
- [87] X. Wang, W. Yao, R. Guo, et al., *Adv. Healthc. Mater.* 7 (14) (2018) e1800318.
- [88] Y. Estrin, N. Martynenko, N. Anisimova, et al., *Materials* 12 (23) (2019).
- [89] T. Li, W. Xu, C. Liu, et al., *ACS Biomater. Sci. Eng.* 7 (6) (2021) 2774–2782.
- [90] R. Hamaguchi, M. Isowa, R. Narui, et al., *Front. Oncol.* 12 (2022) 1003588–1003588.
- [91] Y. Yang, Y. Zhu, X. Xi, *Oncol. Lett.* 16 (3) (2018) 2771–2776.
- [92] N. Veronese, D. Pizzol, L. Smith, et al., *Nutrients* 14 (3) (2022) 679.
- [93] S. Li, R. Liao, X. Sheng, et al., *Front. Oncol.* 9 (2019) 696–696.
- [94] Y. Sun, S. Selvaraj, A. Varma, et al., *J. Biol. Chem.* 288 (1) (2013) 255–263.
- [95] J. Chu, J. Gao, J. Wang, et al., *Oncol. Rep.* 46 (1) (2021).
- [96] Y. Sun, S. Selvaraj, A. Varma, et al., *J. Biol. Chem.* 288 (1) (2013) 255–263.
- [97] F. Saito-Ohara, I. Imoto, J. Inoue, et al., *Cancer Res.* 63 (8) (2003) 1876–1883.
- [98] J. Xie, C.S. Cheng, X.Y. Zhu, et al., *Aging* 11 (9) (2019) 2681–2698.
- [99] M. Royuela, G. Rodríguez-Berriguete, B. Fraile, et al., *Histol. Histopathol.* 23 (10) (2008) 1279–1290.
- [100] D. Bernardini, A. Nasulewic, A. Mazur, et al., *Front. Biosci.* 10 (2005) 1177–1182.
- [101] Y. Jiang, G. Liu, L. Zhang, et al., *Mol. Med. Rep.* 18 (2) (2018) 2182–2190.
- [102] D. Kawai, A. Takaki, A. Nakatsuka, et al., *Hepatology* 56 (3) (2012) 912–921.
- [103] G.D. Liu, H. Zhang, L. Wang, et al., *Int. J. Ophthalmol.* 6 (3) (2013) 280–285.
- [104] H. Kawasaki, J. Guan, K. Tamama, *Biochem. Biophys. Res. Commun.* 397 (3) (2010) 608–613.
- [105] L. Huang, *Med. Gas Res.* 6 (4) (2016) 219–222.
- [106] X. Meng, H. Chen, G. Wang, et al., *Exp. Ther. Med.* 10 (6) (2015) 2277–2282.
- [107] P. Icard, S. Shulman, D. Farhat, et al., *Drug Resist. Updat.* 38 (2018) 1–11.
- [108] A. Tauffenberger, H. Fiumelli, S. Almoustafa, et al., *Cell Death. Dis.* 10 (9) (2019) 653.
- [109] S. Faes, A.P. Duval, A. Planche, et al., *Mol. Cancer* 15 (1) (2016) 78.
- [110] Z. Jin, Y. Lu, X. Wu, et al., *Redox. Biol.* 46 (2021) 102076.
- [111] C.E. Tu, Y. Hu, P. Zhou, et al., *J. Cell. Physiol.* 236 (6) (2021) 4528–4537.
- [112] N.J. Clemons, K.E. Mccoll, R.C. Fitzgerald, *Gastroenterology* 133 (4) (2007) 1198–1209.
- [113] S. Yang, Y. Wang, X. Liang, *Pharmaceutics* 15 (5) (2023).
- [114] S. Gantz, L. Karsch, J. Pawelke, et al., *Proc. Natl. Acad. Sci. U.S.A.* 120 (23) (2023) e2301160120.
- [115] Y. Davatgaran Taghipour, R. Salehi, A. Zarebkohan, et al., *Int. J. Pharm.* (2023) 123095.
- [116] S. Wang, F. Wang, X. Zhao, et al., *Mater. Des.* 217 (2022) 110621.
- [117] P. Globig, R. Willumeit-Romer, F. Martini, et al., *Int. J. Mol. Sci.* 21 (14) (2020).
- [118] O. Hakimi, Y. Ventura, J. Goldman, et al., *Mater. Sci. Eng. C Mater. Biol. Appl.* 61 (2016) 516–525.
- [119] O. Hakimi, E. Aghion, *Adv. Eng. Mater.* 16 (4) (2014) 364–370.
- [120] D. Zhang, R. Xu, S. Chen, et al., *Bioact. Mater.* 30 (2023) 15–28.